Chapter 11

Modelling and Simulation Based Matlab/Simulink of a Strap-Down Inertial Navigation System' Errors due to the Inertial Sensors

Teodor Lucian Grigorie and
Ruxandra Mihaela Botez

Additional information is available at the end of the chapter

http://dx.doi.org/10.5772/57583

1. Introduction

Inertial navigation is a dead reckoning positioning method based on the measurement and mathematical processing of the vehicle absolute acceleration and angular speed in order to estimate its attitude, speed and position related to different reference. Due to the specific operation principle, the positioning errors for this method result from the imperfection of the initial conditions knowledge, from the errors due to the numerical calculation in the inertial system, and from the accelerometers and gyros errors. Therefore, the inertial sensors performances play a main role in the establishment of the navigation system precision, and should be considered in its design phase frames (Bekir, 2007; Farrell, 2008; Grewal et al., 2013; Grigorie, 2007; Salychev, 1998; Titterton and Weston, 2004).

Amazing evolution of physics and manufacturing technologies to improve the optical an electronic fields have made possible the development of opto-electronic rotation and translation sensors in parallel with the mechanical sensors. The Ring Laser Gyros (RLG) have entered the market only in 1980's even if in 1963 was first demonstrated in a square configuration. Mechanical gyroscopes dominated the market and the RLG were required in military applications, because these are ideal systems for high dynamics strap-down inertial navigation, used in extreme environments. The RLG has excellent scale-factor stability and linearity, negligible sensitivity to acceleration, digital output, fast turn-on, excellent stability and repeatability across the range, and no moving parts. Present day RLG's (Ring Laser Gyros) is considered a matured technology and its development efforts are to reduce costs more than

to increase its performance (Barbour & Schmidt, 2001; Barbour et al., 2010; Barbour, 2010; Edu et al., 2011; Hopkins, 2010; Kraft, 2000; Lawrence, 1998).

Fiber optic gyros (FOG) are also a mature technology and were originally designed as a low-cost alternative to the RLG. Surprisingly, today they compete RLG's both in terms of manufacturing costs, as well as that of performance, gaining prominence in a series of military and commercial applications. The studies provide that the developments in solid-state optics and fiber technology could lead to 0.001-deg/h performance in miniature design. Research in the field of fiber optic gyros, similarly to those of RLG, aimed at decreasing the size and manufacturing costs at an approximately constant level of performance, if not better. Development of miniaturized FOGs was based on the technology achievements brought by the telecommunications industry. An important innovation was the discovery of photonic crystal fibers (PCF Fibers crystal photon) that have been a very important step towards the next generation of IFOG instruments, the PC-IFOG. The introduction of PCFs in IFOG applications brings significant advantages to this field, such as the significant reduction of bend losses and fiber size compared to the conventional optical fiber, minimizing the fiber optic coil diameter, the possibility of incorporating a dispersion compensation in the existing PCF, with the effect of reducing the spectral distortion, guiding light through this type of fiber allows the use of a mid-infrared optical wavelength (Barbour & Schmidt, 2001; Divakaruni & Sanders, 2006; Edu et al., 2011; KVH Industries Inc., 2007; Pavlath, 2006; Tawney et al., 2006).

In the 1980s, the Hemispherical Resonant Gyro was developed, a vibratory high performance gyro; the inertial sensing element is a fused-silica hemispherical shell coated with a thin film of metal. HRG advantages are related to the fact that it is very light, compact, operates in vacuum and has no moving parts. Its life cycle is limited only by the electronic components, which are redundant (Barbour & Schmidt, 2001; Barbour, 2010; Edu et al., 2011).

Besides the above mentioned technologies, another technology, very promising in terms of inertial detection, based on atomic interferometry (cold atom inertial sensors) is developing very fast. Atomic interferometry is a sensor-based inertial sensing that uses the atom interferometry, using cold atoms, atoms that are a millionth of a degree above absolute zero, created and then trapped using laser technology. With the researches in optical precision spectroscopy (Nobel Prize 2005) today it is possible to have precise control on the internal and external of freedom of atomic matter. Those huge progresses led to application of ultra-cold matter in fields such as precision measurements, matter wave interferometry and applications in quantum information processing. The atom interferometers are very similar in their basic principle with the optical interferometers. The difference is that the optical wave is replaced with the matter-wave represented by the atoms. The current state-of-art of atom interferometry: the atom interferometers obtained and proof-of-concept. Although, gyros and accelerometers are yet too voluminous, the miniaturization seems feasible in the near future and is developing (Dumke & Mueller, 2010; Edu et al., 2011; Hopkins, 2010; Schmidt, 2010).

The aerospace industry tendencies to realize unmanned aircraft (UAV), micro and nano-satellites, easy to launch in space and with the performances analogous with the actual satellites, imposed a nimble rhythm to the expansion of the NEMS (Nano-Electro-Mechanical-Systems) and MEMS (Micro-Electro-Mechanical-Systems) technologies in the domain of the

http://dx.doi.org/10.5772/57583

acceleration and rotation sensors, used especially in the inertial navigation systems. The use of such miniaturized sensors creates the premises to have redundant strap-down inertial navigation systems through the miscellaneous dedicated architectures and at the low-costs comparatively with the case of non-miniaturized and very precise inertial sensors use. On the other way, the use of these miniaturization technologies for the inertial sensors allows the implementation of the entire inertial navigation system in a single chip, including here the sensors and all circuits for the signals conditioning (Bose, 2008; Grewal et al., 2013; Grigorie, 2006; Grigorie et al., 2012 a; Titterton and Weston, 2004).

From the other point of view, these miniaturized sensors have some disadvantages due to the performances decrease with the miniaturization degree increase. They are quite noises, because at the great majority of the acceleration sensors the noise density is between 100 $\mu g/Hz^{1/2}$ and a few hundreds of $\mu g/Hz^{1/2}$, for the bandwidths between 100Hz and 2500Hz, and at the gyro sensors it is between 0.001 $(^o/s)/Hz^{1/2}$ and 0.1 $(^o/s)/Hz^{1/2}$, for the pass bandwidths between 50Hz and 100Hz. Also, for the same type of sensors the noise density can vary from one sensor to the other with 20% of the catalogue value. The filtering of the noise it is not recommended because it is possible to be altered the useful signal and, so, the sensor output doesn't reflect exactly the signal applied at the input of the sensor. Beside the noise increase, through miniaturization appear negative influences on the stability and value of bias, on the scale factor calibration, on the cross-axis sensitivity for the accelerometers and on the sensitivity at the accelerations applied along any given axis for the gyros. For all of these the data sheets of the MEMS and NEMS products stipulate maximal values relatively high, without be able to specify exactly their value to be corrected (Grigorie et al., 2010 a; Grigorie et al., 2010 b).

To test the influences of the sensors errors on the solution of navigation of strap-down inertial navigators we realized Matlab/Simulink models for the acceleration and rotation sensors based on the sensors data sheets and on the IEEE equivalent models for the inertial sensors (Grigorie et al., 2010 a; Grigorie et al., 2010 b). For example, for the accelerometers was obtained the model in Figure 1. He has as inputs the acceleration a_i, applied along of the sensitive axis, and the cross-axis acceleration a_c, and as output the perturbed acceleration a (Grigorie et al., 2010 a). The analytic form of the model is:

$$a = (a_i + Na_i + B + k_c a_c + \nu)(1 + \Delta K / K); \tag{1}$$

N is sensitivity axis misalignment (in radians), B-bias (expressed in percent of span), k_c-cross-axis sensitivity (expressed in percent of a_c), ν-sensor noise (given by its density ν_d expressed in $\mu g/Hz^{1/2}$, K-scale factor (expressed in mV/g), and ΔK-scale factor error (percents of K), and a, a_i, a_c expressed in m/s^2. The model was built for few miniaturized acceleration sensors and covers theirs main errors: bias, scale factor error, sensitivity axis misalignment, cross axis sensitivity and noise.

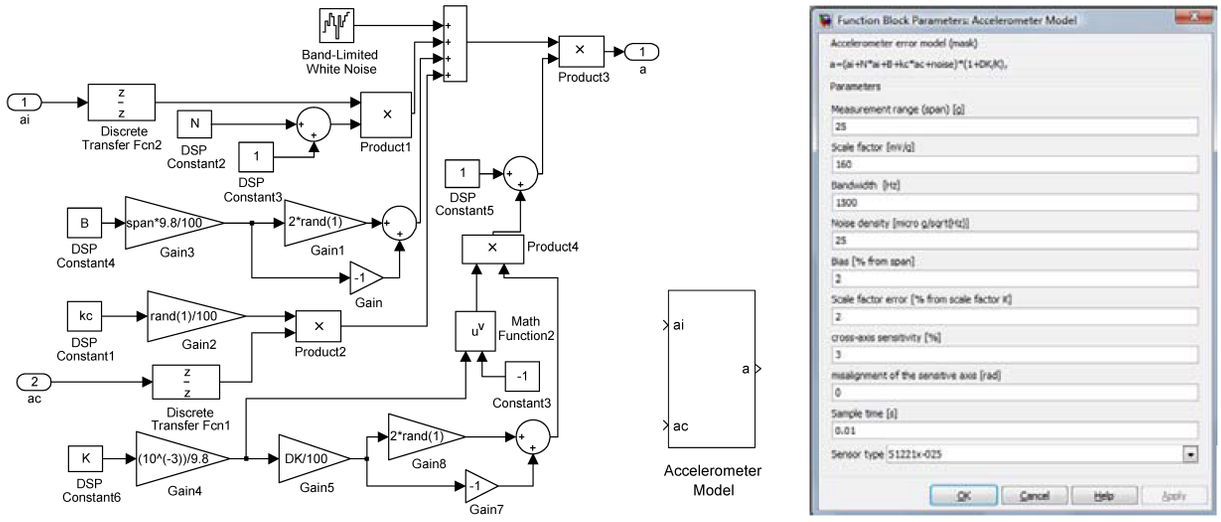

Figure 1. Accelerometers Matlab/Simulink model and its interface.

The model related to the gyro sensors was implemented in Matlab/Simulink (Figure 2) starting from the equation (Grigorie et al., 2010 b):

$$\omega = (\omega_i + S \cdot a_r + B + \nu)(1 + \Delta K / K); \tag{2}$$

ω-sensors output angular speed (disturbed signal) expressed in °/s, ω_i-applied angular speed (°/s), *S*-sensitivity to the acceleration a_r applied on an arbitrary direction ((°/s)/*g*), *B*-bias (expressed in percents of span), ν-sensor noise (given by its density ν_d expressed in (°/s)/Hz$^{1/2}$), *K*-scale factor (expressed in mV/(°/s)), Δ*K*-scale factor error (percents of *K*).

For both models, the change of the sensor type that will be used in simulations is made using the associated interfaces. In addition, the interfaces allow the setting of the models, by the user, in custom variants. The models have the advantages to work independent with each of the sensor errors and to study in this way their influence on the inertial navigator positioning solution. Although sensors data sheets specifications are not related to the components of noise, for a more detailed study of the navigators' errors, the sensors' models can be completed with some noise terms starting from theirs Allan variance definitions. Allan's variance results are related to the seven noise terms. Five noise terms are basic terms: angle random walk, rate random walk, bias instability, quantization noise and drift rate ramp, while the other two are the sinusoidal noise and exponentially correlated (Markov) noise (Grigorie et al., 2010 c; Grigorie et al., 2012 b).

This chapter deals with solving of a navigation problem relative to terrestrial non-inertial reference frames by using attitude matrices to calculate the vehicle attitude. Once it is highlighted the general equation of inertial navigation, a numerical algorithm is developed for determining the position and speed of the vehicle based on this equation. The algorithm provides position and vehicle speed in horizontal local reference frame (ENU) and its global

http://dx.doi.org/10.5772/57583

coordinates (latitude, longitude and altitude). For the presented algorithm is developed an error model that highlights the dependencies of the vehicle positioning, velocity and attitude errors by the strap-down inertial sensor errors used to detect acceleration and angular speed. In the development of the error model the small perturbation technique is used. Following is conducted a study of the dependence of the inertial navigator outputs errors by the errors of the used inertial sensors based on the Matlab/Simulink models built for acceleration and gyro sensors.

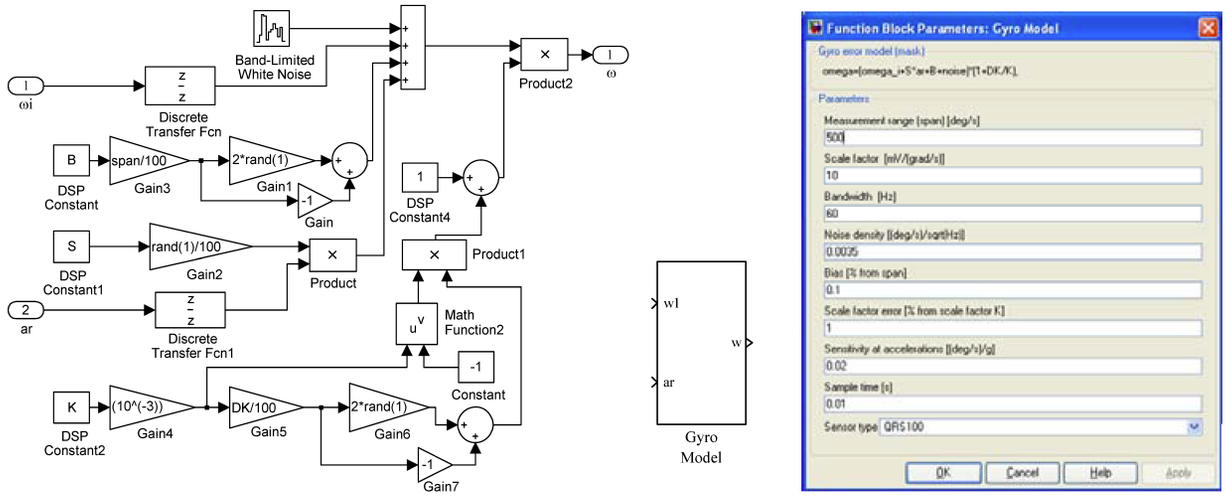

Figure 2. Gyros Matlab/Simulink model and its interface.

2. Navigation algorithm

The output $\vec{f}$ of an accelerometer is influenced by the gravitational field, it being a combination between the vehicle kinematic acceleration $\vec{a}$ and the gravitational acceleration $\vec{g}$, i.e. $\vec{f} = \vec{a} - \vec{g}$. In literature, f is very well known as specific force (Farrell, 2008; Titterton and Weston, 2004).

On the other way, according to the Coriolis formula we have:

$$\left.\frac{\mathrm{d}\vec{r}}{\mathrm{d}t}\right|_I = \left.\frac{\mathrm{d}\vec{r}}{\mathrm{d}t}\right|_P + \vec{\Omega}\times\vec{r} = \vec{v} + \vec{\Omega}\times\vec{r}, \tag{3}$$

from where it results:

$$\vec{a} = \frac{\mathrm{d}}{\mathrm{d}t}\left[\left.\frac{\mathrm{d}\vec{r}}{\mathrm{d}t}\right|_I\right]_I = \frac{\mathrm{d}}{\mathrm{d}t}\left[\vec{v} + \vec{\Omega}\times\vec{r}\right]_I = \left.\frac{\mathrm{d}\vec{v}}{\mathrm{d}t}\right|_I + \vec{\Omega}\times\left.\frac{\mathrm{d}\vec{r}}{\mathrm{d}t}\right|_I = \left.\frac{\mathrm{d}\vec{v}}{\mathrm{d}t}\right|_I + \vec{\Omega}\times\vec{v} + \vec{\Omega}\times\left(\vec{\Omega}\times\vec{r}\right); \tag{4}$$

$\vec{r}$ is the position vector of the monitored vehicle in inertial frame *I*, $\vec{v}$-the vehicle speed relative to the ECEF (Earth Centered Earth Fixed) reference frame (denoted with *P*), and $\vec{\Omega}$-Earth rotation speed around its axis.

Denoting with $\vec{\omega}_N$ the absolute angular speed of the navigation reference frame *N*, then the Coriolis formula applied to the $(\mathrm{d}\vec{v}/\mathrm{d}t)|_I$ term implies:

$$\left.\frac{\mathrm{d}\vec{v}}{\mathrm{d}t}\right|_I = \left.\frac{\mathrm{d}\vec{v}}{\mathrm{d}t}\right|_N + \vec{\omega}_N \times \vec{v}, \tag{5}$$

where $(\mathrm{d}\vec{v}/\mathrm{d}t)_N$ is the derivative of $\vec{v}$ relative to the navigation frame. Therefore, the acceleration $\vec{a}$ becomes:

$$\vec{a} = \left.\frac{\mathrm{d}\vec{v}}{\mathrm{d}t}\right|_N + \vec{\omega}_N \times \vec{v} + \vec{\Omega} \times \vec{v} + \vec{\Omega} \times \left(\vec{\Omega} \times \vec{r}\right), \tag{6}$$

and the specific force can be rewritten as:

$$\vec{f} = \left.\frac{\mathrm{d}\vec{v}}{\mathrm{d}t}\right|_N + \vec{\omega}_N \times \vec{v} + \vec{\Omega} \times \vec{v} + \vec{\Omega} \times \left(\vec{\Omega} \times \vec{r}\right) - \vec{g}. \tag{7}$$

Considering the expression $\vec{g}_a = \vec{g} - \vec{\Omega} \times (\vec{\Omega} \times \vec{r})$ for the apparent gravitational acceleration, eq. (7) implies:

$$\vec{f} = \left.\frac{\mathrm{d}\vec{v}}{\mathrm{d}t}\right|_N + \vec{\omega}_N \times \vec{v} + \vec{\Omega} \times \vec{v} - \vec{g}_a, \tag{8}$$

which is known as general equation of the inertial navigation.

The position and the speed of a vehicle may be obtained by the numerical integration of the eq. (8) relative to the navigation frame (Farrell, 2008; Salychev, 1998; Titterton and Weston, 2004). In the inertial navigation systems with stable platform, the axes of the acceleration sensors are kept parallel with the navigation frame axes, and, as a consequence, the components of the specific force are obtained directly in this frame. If a strap-down architecture is used for the inertial measurement unit (IMU), then the components of the specific force in the navigation frame should be calculated starting from the specific force components in the vehicle frame (SV); the acceleration sensors in IMU are fixed directly on the vehicle rigid structure. In this situation the coordinate change between the vehicle frame and navigation

http://dx.doi.org/10.5772/57583

frame is made by using the rotation matrix describing the vehicle attitude relative to the navigation frame.

By choosing as navigation frame the local horizontal frame ENU (East-North-Up) it results $\vec{\omega}_N = \vec{\omega}_l$ (index l denotes the ENU frame). The scalar components of the eq. (8) in this frame are:

$$\begin{aligned} f_{xl} &= \frac{\mathrm{d}v_{xl}}{\mathrm{d}t} + \omega_{yl}v_{zl} - \omega_{zl}v_{yl} + \Omega_{yl}v_{zl} - \Omega_{zl}v_{yl} - g_{axl}, \\ f_{yl} &= \frac{\mathrm{d}v_{yl}}{\mathrm{d}t} - \omega_{xl}v_{zl} + \omega_{zl}v_{xl} - \Omega_{xl}v_{zl} + \Omega_{zl}v_{xl} - g_{ayl}, \\ f_{zl} &= \frac{\mathrm{d}v_{zl}}{\mathrm{d}t} + \omega_{xl}v_{yl} - \omega_{yl}v_{xl} + \Omega_{xl}v_{yl} - \Omega_{yl}v_{xl} - g_{azl}, \end{aligned} \tag{9}$$

where f_{xl}, f_{yl}, f_{zl} are the components of the specific force in ENU frame; v_{xl}, v_{yl}, v_{zl}-components of the vehicle speed relative to ECEF frame in ENU frame; ω_{xl}, ω_{yl}, ω_{zl}-components of the ENU frame absolute angular speed $\vec{\omega}_l$ on its own axes; Ω_{xl}, Ω_{yl}, Ω_{zl}-components of $\vec{\Omega}$ in ENU frame; g_{axl}, g_{ayl}, g_{azl}-components of the apparent gravitational acceleration in ENU frame (Farrell, 2008; Grigorie, 2007; Radix, 1993):

$$g_{xl} \cong 0,\ g_{yl} \cong 0,\ g_{zl} \cong 9{,}7803 + 0{,}0519 \cdot \sin^2\phi - 3{,}08 \cdot 10^{-6} \cdot h. \tag{10}$$

With these considerations we have (Farrell, 2008; Grigorie, 2007; Radix, 1993):

$$\left[\vec{\Omega}\right]_l = \begin{bmatrix} \Omega_{xl} & \Omega_{yl} & \Omega_{zl} \end{bmatrix}^T = \begin{bmatrix} 0 & \Omega\cos\phi & \Omega\sin\phi \end{bmatrix}^T, \tag{11}$$

$$\left[\vec{\omega}_l\right]_l = [\omega_{xl},\ \omega_{yl},\ \omega_{zl}]^T = \left[-\frac{v_{yl}}{R_\phi + h},\ \frac{v_{xl}}{R_\lambda + h} + \Omega\cos\phi,\ \frac{v_{xl}}{R_\lambda + h}\mathrm{tg}\phi + \Omega\sin\phi \right]^T, \tag{12}$$

h is the altitude relative to the reference ellipsoid, R_ϕşi R_λ-principal radii of curvature of the reference ellipsoid (Farrell, 2008; Grigorie, 2007; Radix, 1993):

$$R_\phi = a\frac{1-e^2}{(1-e^2\sin^2\phi)^{3/2}},\ R_\lambda = \frac{a}{(1-e^2\sin^2\phi)^{1/2}}, \tag{13}$$

λ and ϕ are the longitude and the latitude. The angular speed $\vec{\omega}_r$, relative to the ECEF reference frame, has in ENU frame the next components:

$$\left[\vec{\omega}_r\right]_l = [\omega_{rxl},\ \omega_{ryl},\ \omega_{rzl}]^T = \left[-\frac{v_{yl}}{R_\phi + h},\ \frac{v_{xl}}{R_\lambda + h},\ \frac{v_{xl}}{R_\lambda + h}\mathrm{tg}\phi\right]^T. \tag{14}$$

Therefore, equations (9) become:

$$\begin{aligned}
\frac{\mathrm{d}v_{xl}}{\mathrm{d}t} &= f_{xl} + \frac{v_{xl}v_{yl}}{R_\lambda + h}\mathrm{tg}\phi + 2\Omega\sin\phi v_{yl} - v_{zl}\left(\frac{v_{xl}}{R_\lambda + h} + 2\Omega\cos\phi\right) + g_{axl},\\
\frac{\mathrm{d}v_{yl}}{\mathrm{d}t} &= f_{yl} - \frac{v_{xl}^2}{R_\lambda + h}\mathrm{tg}\phi - 2\Omega\sin\phi v_{xl} - v_{zl}\frac{v_{yl}}{R_\phi + h} + g_{ayl},\\
\frac{\mathrm{d}v_{zl}}{\mathrm{d}t} &= f_{zl} + \frac{v_{yl}^2}{R_\phi + h} + \frac{v_{xl}^2}{R_\lambda + h} + 2\Omega v_{xl}\cos\phi + g_{azl}.
\end{aligned} \tag{15}$$

To integrate these equations we need to know the initial values of ϕ, λ, h, v_{xl}, v_{yl}, v_{zl}, and, also, the components of $\vec{f}$ and $\vec{g}$ in ENU frame. Because the IMU of the strap-down inertial navigation system contains three accelerometers and three gyros, its inputs will be the components of the vehicle absolute acceleration and angular speed in the vehicle frame:

$$[\vec{f}]_v = [f_{xv},\ f_{yv},\ f_{zv}]^T, \tag{16}$$

$$[\vec{\omega}_v]_v = [\omega_{xv},\ \omega_{yv},\ \omega_{zv}]^T. \tag{17}$$

The components of the specific force in ENU can be determinate by using the relation:

$$[\vec{f}]_l = R_v^l[\vec{f}]_v, \tag{18}$$

where R_v^l is the rotation matrix performing the coordinate change between SV frame and ENU frame and can be calculated by solving the next Poisson equation (Farrell, 2008):

$$\dot{R}_v^l = R_v^l\tilde{\omega}_v - \tilde{\omega}_l R_v^l. \tag{19}$$

In eq. (19) $\tilde{\omega}_v$ and $\tilde{\omega}_l$ have the expressions:

http://dx.doi.org/10.5772/57583

$$\tilde{\omega}_v = \begin{bmatrix} 0 & -\omega_{zv} & \omega_{yv} \\ \omega_{zv} & 0 & -\omega_{xv} \\ -\omega_{yv} & \omega_{xv} & 0 \end{bmatrix}, \tilde{\omega}_l = \begin{bmatrix} 0 & -\omega_{zl} & \omega_{yl} \\ \omega_{zl} & 0 & -\omega_{xl} \\ -\omega_{yl} & \omega_{xl} & 0 \end{bmatrix}. \tag{20}$$

Can be easily observed that eq. (19) has the general form:

$$\dot{X} = XA - BX, \tag{21}$$

with $A = \tilde{\omega}_v$ and $B = \tilde{\omega}_l$. Considering that for a short period of time Δt, between t_n and t_{n+1} times, the angular speeds ω_{xv}, ω_{yv}, ω_{zv} and ω_{xl}, ω_{yl}, ω_{zl} are constant, we obtains:

$$\Delta\phi_{xv} = \int_{t_n}^{t_{n+1}} \omega_{xv} \mathrm{d}t = \omega_{xv}\Delta t,\ \Delta\phi_{yv} = \int_{t_n}^{t_{n+1}} \omega_{yv} \mathrm{d}t = \omega_{yv}\Delta t,\ \Delta\phi_{zv} = \int_{t_n}^{t_{n+1}} \omega_{zv} \mathrm{d}t = \omega_{zv}\Delta t \tag{22}$$

and

$$\Delta\phi_{xl} = \int_{t_n}^{t_{n+1}} \omega_{xl} \mathrm{d}t = \omega_{xl}\Delta t,\ \Delta\phi_{yl} = \int_{t_n}^{t_{n+1}} \omega_{yl} \mathrm{d}t = \omega_{yl}\Delta t,\ \Delta\phi_{zl} = \int_{t_n}^{t_{n+1}} \omega_{zl} \mathrm{d}t = \omega_{zl}\Delta t. \tag{23}$$

$\Delta\phi_{xv}$, $\Delta\phi_{yv}$, $\Delta\phi_{zv}$, respectively $\Delta\phi_{xl}$, $\Delta\phi_{yl}$, $\Delta\phi_{zl}$ are the increments of the angular rotations measured around the roll, pitch and yaw axes, respectively the increments of the angular rotations around the ENU frame axes calculated by the navigation processor. In this way, the value provided for the X matrix at the t_{n+1} time is given by:

$$X_{n+1} = X_n + \dot{X}_n\Delta t = X_n + X_n A\Delta t - B\Delta t X_n, \tag{24}$$

from where it is obtained:

$$X_{n+1} = X_n(I + A\Delta t) - B\Delta t X_n = X_n A_n - B_n X_n, \tag{25}$$

with:

$$A_n = \begin{bmatrix} 1 & -\Delta\phi_{zv} & \Delta\phi_{yv} \\ \Delta\phi_{zv} & 1 & -\Delta\phi_{xv} \\ -\Delta\phi_{yv} & \Delta\phi_{xv} & 1 \end{bmatrix}, B_n = \begin{bmatrix} 0 & -\Delta\phi_{zl} & \Delta\phi_{yl} \\ \Delta\phi_{zl} & 0 & -\Delta\phi_{xl} \\ -\Delta\phi_{yl} & \Delta\phi_{xl} & 0 \end{bmatrix}. \tag{26}$$

Therefore, the solution of the eq. (19) has the form:

$$R_v^l\Big|_{n+1} = R_v^l\Big|_n A_n - B_n R_v^l\Big|_n . \tag{27}$$

Through the numerical integration of the equations (15) are obtained the components of the relative speed $\vec{v}$ in ENU frame:v_{xl}, v_{yl}, v_{zl}. With the equations (Salychev, 1998):

$$\begin{aligned} \dot{\phi} &= \frac{v_{yl}}{R_\phi + h}, \\ \dot{\lambda} &= \frac{v_{xl}}{\left(R_\lambda + h\right)\cos\phi}, \\ \dot{h} &= v_{zl}. \end{aligned} \tag{28}$$

it result the geographic coordinated of the vehicle:

$$\begin{aligned} \phi(t) &= \phi(0) + \int_0^t \frac{v_{yl}}{R_\phi + h}\mathrm{d}t, \\ \lambda(t) &= \lambda(0) + \int_0^t \frac{v_{xl}}{\left(R_\lambda + h\right)\cos\phi}\mathrm{d}t, \\ h(t) &= h(0) + \int_0^t v_{zl}\mathrm{d}t. \end{aligned} \tag{29}$$

By using the rotation matrix between ENU and ECEF frames (Farrell, 2008; Salychev, 1998; Titterton and Weston, 2004):

$$[R_l^P]^T = R_P^l = \begin{bmatrix} -\sin\lambda & \cos\lambda & 0 \\ -\sin\phi\cos\lambda & -\sin\phi\sin\lambda & \cos\phi \\ \cos\phi\cos\lambda & \cos\phi\sin\lambda & \sin\phi \end{bmatrix} \tag{30}$$

the components of the relative speed $\vec{v}$ in ECEF frame result with equation:

$$[\vec{v}]_P = R_l^P [\vec{v}]_l. \tag{31}$$

By numerical integration of the relative speed $[\vec{v}]_P$ is obtained $[\vec{r}]_P$:

http://dx.doi.org/10.5772/57583

$$[\vec{r}]_P = [\vec{r}(0)]_P + \int_0^t [\vec{v}]_P \mathrm{d}t = [x_P \; y_P \; z_P]^T, \tag{32}$$

from which, with the model of the gravitational field for ECEF reference frame (Radix, 1993), it results:

$$[\vec{g}_a]_P = \begin{bmatrix} g_{aX^P} \\ g_{aY^P} \\ g_{aZ^P} \end{bmatrix} = \begin{bmatrix} A_1 \frac{x_P}{r^3}\left(1 + \frac{A_2}{r^2}\left(\frac{5z_P^2}{r^2} - 1\right)\right) + \Omega^2 \cdot x_P \\ A_1 \frac{y_P}{r^3}\left(1 + \frac{A_2}{r^2}\left(\frac{5z_P^2}{r^2} - 1\right)\right) + \Omega^2 \cdot y_P \\ A_1 \frac{z_P}{r^3}\left(1 + \frac{A_2}{r^2}\left(\frac{5z_P^2}{r^2} - 3\right)\right) \end{bmatrix}; \tag{33}$$

$A_1 = -3,\, 986005 \cdot 10^{14}\, \mathrm{m}^3/\mathrm{s}^2$, $A_2 = -6,\, 66425 \cdot 10^{10}\, \mathrm{m}^2$ (Radix, 1993). Components of $\vec{g}_a$ in ENU frame, starting from the model (33), are calculated by using the inverse transform ECEF to ENU:

$$[\vec{g}_a]_l = R_P^l [\vec{g}_a]_P. \tag{34}$$

Finally, the vehicle coordinates in ENU are obtained with the equation:

$$[\vec{r}']_l = [\vec{r}'(0)]_l + \int_0^t [\vec{v}]_l \mathrm{d}t = [x_l \; y_l \; z_l]^T, \tag{35}$$

where $\vec{r}'$ is the vehicle position vector in ENU reference frame. From the mathematical description of the algorithm, it results the block diagram in Fig. 3.

3. Error model of the navigation algorithm

The quality of the inertial navigator depends by the precision of the used sensors and by the numerical algorithms implemented in the navigation processor. For the error model developed in this subchapter are taken into account only the errors of the inertial sensors, considering that the numerical algorithm implemented in the navigation processor works free of errors. Thus, the model highlights the dependence of the position, velocity and attitude errors by the errors of the accelerometers and gyros in strap-down IMU. In the development of the error

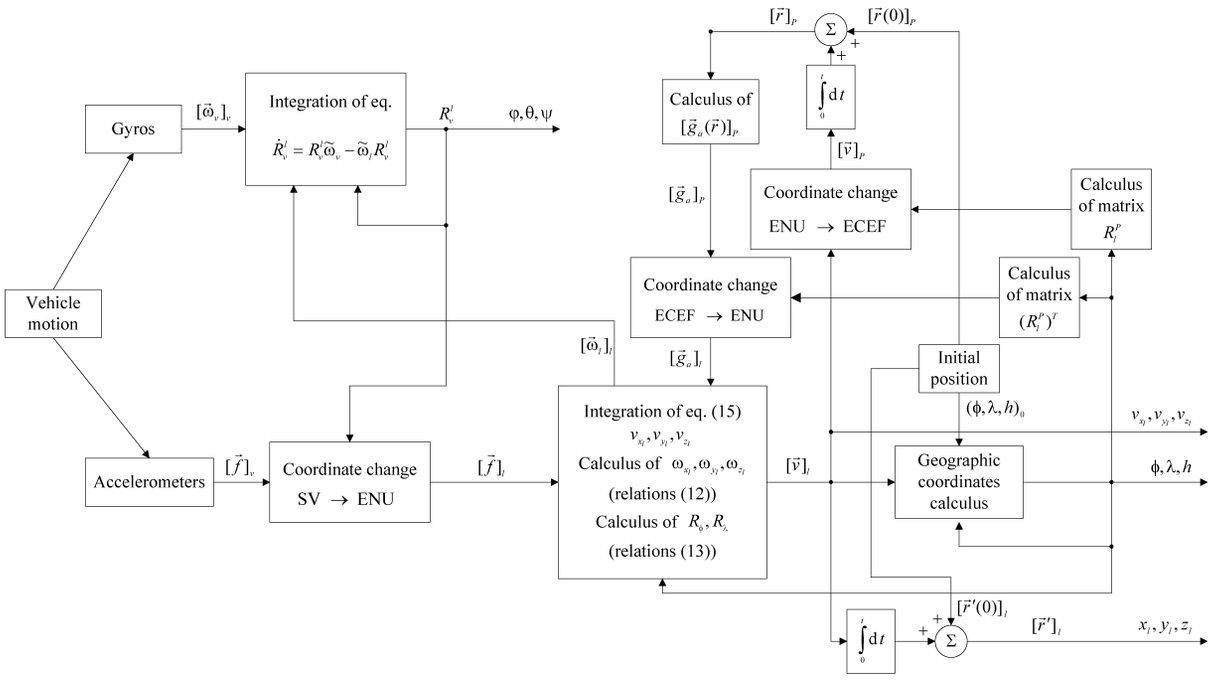

Figure 3. Block diagram of the navigation algorithm.

model are used techniques widely presented in the literature (Dahia, 2005; Farrell, 2008; Salychev, 1998; Savage, 2000).

Denoting with m the ideal value of a measurement and with $\widehat{m}$ its real value, given by the measurement system, the measurement error is calculated with the relation:

$$\delta m = m - \widehat{m}. \tag{36}$$

Starting from this expression, and having in mind that accelerometric readings are denoted with f_{xv}, f_{yv}, f_{zv}, and gyro readings are denoted with ω_{xv}, ω_{yv}, ω_{zv}, it result the errors of the accelerometric and gyro sensors under the scalar forms (the components for all three IMU axes):

$$\delta f_{xv} = f_{xv} - \widehat{f}_{xv},\ \delta f_{yv} = f_{yv} - \widehat{f}_{yv},\ \delta f_{zv} = f_{yv} - \widehat{f}_{yv}, \tag{37}$$

$$\delta \omega_{xv} = \omega_{xv} - \widehat{\omega}_{xv},\ \delta \omega_{yv} = \omega_{yv} - \widehat{\omega}_{yv},\ \delta \omega_{zv} = \omega_{zv} - \widehat{\omega}_{zv} \tag{38}$$

and, under the vector forms:

http://dx.doi.org/10.5772/57583

$$\delta\vec{f} = \vec{f} - \hat{\vec{f}}, \tag{39}$$

$$\delta\vec{\omega}_v = \vec{\omega}_v - \hat{\vec{\omega}}_v. \tag{40}$$

Similarly can be defined the errors of the attitude angles (φ, θ, ψ-roll, pitch and yaw), the errors of the vehicle position over the ENU frame axes (x_l, y_l, z_l), and the errors of the vehicle linear speed (v_{xl}, v_{yl}, v_{zl}):

$$\delta\varphi = \varphi - \hat{\varphi},\ \delta\theta = \theta - \hat{\theta},\ \delta\psi = \psi - \hat{\psi}, \tag{41}$$

$$\begin{aligned} &\delta x_l = x_l - \hat{x}_l,\ \delta y_l = y_l - \hat{y}_l,\ \delta z_l = z_l - \hat{z}_l, \\ &\delta\vec{r}' = \vec{r}' - \hat{\vec{r}}'. \end{aligned} \tag{42}$$

$$\begin{aligned} &\delta v_{xl} = v_{xl} - \hat{v}_{xl},\ \delta v_{yl} = v_{yl} - \hat{v}_{yl},\ \delta v_{zl} = v_{zl} - \hat{v}_{zl}, \\ &\delta\vec{v} = \vec{v} - \hat{\vec{v}}. \end{aligned} \tag{43}$$

Starting from the errors of the attitude angles may be deduced the errors affecting the attitude matrices. Thus, with the equations expressing the elements of the rotation matrix R_l^v (ENU to SV) (Farrell, 2008; Salychev, 1998; Titterton and Weston, 2004) and considering as negligible the products of the attitude angles errors taken as small perturbations, ($\delta\varphi \cdot \delta\theta = \delta\varphi \cdot \delta\psi = \delta\theta \cdot \delta\psi = 0$), it results:

$$R_l^v = \hat{R}_l^v \begin{bmatrix} 1 & -\delta\psi & \delta\theta \\ \delta\psi & 1 & -\delta\varphi \\ -\delta\theta & \delta\varphi & 1 \end{bmatrix} = \hat{R}_l^v (I_3 + \tilde{R}),\ \text{with}\ \tilde{R} = \begin{bmatrix} 0 & -\delta\psi & \delta\theta \\ \delta\psi & 0 & -\delta\varphi \\ -\delta\theta & \delta\varphi & 0 \end{bmatrix}, \tag{44}$$

where R_l^v is the right matrix, and $\overset{\frown}{R}_l^v$-the matrix provided by the navigation system. From eq. (44) we have:

$$R_v^l = (R_l^v)^T = (I_3 + \tilde{R})^T \cdot (\hat{R}_l^v)^T = (I_3 - \tilde{R}) \cdot \hat{R}_v^l. \tag{45}$$

In similar way, for the R_P^l matrix (ECEF to ENU) (Farrell, 2008; Salychev, 1998; Titterton and Weston, 2004), in which are considered the latitude and longitude errors:

$$\delta\lambda = \lambda - \hat{\lambda},\ \delta\phi = \phi - \hat{\phi}, \tag{46}$$

it results:

$$R_P^l = (I_3 - \tilde{P}) \cdot \hat{R}_P^l, \tag{47}$$

where R_P^l is the right matrix, $\overset{\frown}{R}{}_P^l$-the matrix provided by the navigation system, and $\tilde{P}$ has the form:

$$\tilde{P} = \begin{bmatrix} 0 & -\delta p_z & \delta p_y \\ \delta p_z & 0 & -\delta p_x \\ -\delta p_y & \delta p_x & 0 \end{bmatrix} \tag{48}$$

with:

$$\delta p_x = -\delta\phi,\ \delta p_y = \cos\hat{\phi} \cdot \delta\lambda,\ \delta p_z = \sin\hat{\phi} \cdot \delta\lambda. \tag{49}$$

One of the form of the attitude Poisson equation is (Farrell, 2008; Grigorie, 2007; Salychev, 1998; Titterton and Weston, 2004):

$$\dot{R}_l^v = R_l^v \cdot \tilde{\omega}_l - \tilde{\omega}_v \cdot R_l^v, \tag{50}$$

where $\tilde{\omega}_l$ and $\tilde{\omega}_v$ have the expressions given by equations (20). Due to the erroneous measurements, the inertial system integrates the next equation:

$$\dot{\hat{R}}_l^v = \hat{R}_l^v \cdot \tilde{\hat{\omega}}_l - \tilde{\hat{\omega}}_v \cdot \hat{R}_l^v. \tag{51}$$

Thus, it results:

$$\dot{\hat{R}}_l^v = \hat{R}_l^v \cdot (\tilde{\omega}_l - \delta\tilde{\omega}_l) - (\tilde{\omega}_v - \delta\tilde{\omega}_v) \cdot \hat{R}_l^v, \tag{52}$$

with

http://dx.doi.org/10.5772/57583

$$\delta\tilde{\omega}_v = \begin{bmatrix} 0 & -\delta\omega_{zv} & \delta\omega_{yv} \\ \delta\omega_{zv} & 0 & -\delta\omega_{xv} \\ -\delta\omega_{yv} & \delta\omega_{xv} & 0 \end{bmatrix},\ \delta\tilde{\omega}_l = \begin{bmatrix} 0 & -\delta\omega_{zl} & \delta\omega_{yl} \\ \delta\omega_{zl} & 0 & -\delta\omega_{xl} \\ -\delta\omega_{yl} & \delta\omega_{xl} & 0 \end{bmatrix}. \tag{53}$$

From (44) we obtain:

$$R_l^v - \hat{R}_l^v = \hat{R}_l^v \cdot \tilde{R}, \tag{54}$$

which, through derivation, implies:

$$\dot{R}_l^v - \dot{\hat{R}}_l^v = \dot{\hat{R}}_l^v \cdot \tilde{R} + \hat{R}_l^v \cdot \dot{\tilde{R}}, \tag{55}$$

i.e.

$$\hat{R}_l^v \cdot \dot{\tilde{R}} = \dot{R}_l^v - \dot{\hat{R}}_l^v \cdot (I_3 + \tilde{R}). \tag{56}$$

Substituting relations (50) and (52) in (56), get to the formula:

$$\hat{R}_l^v \cdot \dot{\tilde{R}} = \hat{R}_l^v \cdot \tilde{R} \cdot \tilde{\omega}_l - \hat{R}_l^v \cdot \tilde{\omega}_l \cdot \tilde{R} + (\hat{R}_l^v \cdot \delta\tilde{\omega}_l - \delta\tilde{\omega}_v \cdot \hat{R}_l^v)(I_3 + \tilde{R}). \tag{57}$$

Considering expressions of $\tilde{R}$, $\delta\tilde{\omega}_v$ and$\delta\tilde{\omega}_l$, in formula (57) can be neglected the products between small quantities ($\overset{\frown}{R}_l^v \cdot \delta\tilde{\omega}_l \cdot \tilde{R}and\delta\tilde{\omega}_v \cdot \overset{\frown}{R}_l^v \cdot \tilde{R}$) and we obtain:

$$\hat{R}_l^v \cdot \dot{\tilde{R}} = \hat{R}_l^v \cdot \tilde{R} \cdot \tilde{\omega}_l - \hat{R}_l^v \cdot \tilde{\omega}_l \cdot \tilde{R} + \hat{R}_l^v \cdot \delta\tilde{\omega}_l - \delta\tilde{\omega}_v \cdot \hat{R}_l^v, \tag{58}$$

which, by multiplication on the left with$(\overset{\frown}{R}_l^v)^T$, leads to the relation:

$$\dot{\tilde{R}} = \tilde{R} \cdot \tilde{\omega}_l - \tilde{\omega}_l \cdot \tilde{R} + \delta\tilde{\omega}_l - (\hat{R}_l^v)^T \cdot \delta\tilde{\omega}_v \cdot \hat{R}_l^v. \tag{59}$$

With formulas (12) and (28) it results:

$$\left[\vec{\omega}_l\right]_l = [\omega_{xl},\ \omega_{yl},\ \omega_{zl}]^T = \left[-\dot{\phi},\ \dot{\lambda}\cos\phi + \Omega\cos\phi,\ \dot{\lambda}\sin\phi + \Omega\sin\phi\right]^T, \tag{60}$$

Evaluating the terms of differential equation (59), we obtain:

$$\tilde{R}\cdot\tilde{\omega}_l-\tilde{\omega}_l\cdot\tilde{R}=\begin{bmatrix}0 & -(\omega_{yl}\delta\phi-\omega_{xl}\delta\theta) & \omega_{xl}\delta\psi-\omega_{zl}\delta\phi\\ \omega_{yl}\delta\phi-\omega_{xl}\delta\theta & 0 & -(\omega_{zl}\delta\theta-\omega_{yl}\delta\psi)\\ -(\omega_{xl}\delta\psi-\omega_{zl}\delta\phi) & \omega_{zl}\delta\theta-\omega_{yl}\delta\psi & 0\end{bmatrix}, \tag{61}$$

$$[\delta\vec{\omega}_l]_l=\begin{bmatrix}\delta\omega_{xl}\\ \delta\omega_{yl}\\ \delta\omega_{zl}\end{bmatrix}=\begin{bmatrix}-\delta\dot{\phi}\\ -\sin\phi\cdot\dot{\lambda}\cdot\delta\phi+\cos\phi\cdot\delta\dot{\lambda}-\Omega\cdot\sin\phi\cdot\delta\phi\\ \cos\phi\cdot\dot{\lambda}\cdot\delta\phi+\sin\phi\cdot\delta\dot{\lambda}+\Omega\cdot\cos\phi\cdot\delta\phi\end{bmatrix}, \tag{62}$$

and for the product $(\overset{\frown}{R}_l^{\,v})^{T}\cdot\delta\tilde{\omega}_v\cdot\overset{\frown}{R}_l^{\,v}$ the resulting matrix elements are given by the expressions:

$$\begin{aligned}
&a_{11}=a_{22}=a_{33},\\
&a_{21}=-a_{12}=-\sin\hat{\theta}\cdot\delta\omega_{xv}+\sin\hat{\phi}\cos\hat{\theta}\cdot\delta\omega_{yv}+\cos\hat{\phi}\cos\hat{\theta}\cdot\delta\omega_{zv},\\
&a_{13}=-a_{31}=\cos\hat{\theta}\sin\hat{\psi}\cdot\delta\omega_{xv}+(\sin\hat{\phi}\sin\hat{\theta}\sin\hat{\psi}+\cos\hat{\phi}\cos\hat{\psi})\cdot\delta\omega_{yv}+\\
&\qquad+(\cos\hat{\phi}\sin\hat{\theta}\sin\hat{\psi}-\sin\hat{\phi}\cos\hat{\psi})\cdot\delta\omega_{zv},\\
&a_{32}=-a_{23}=\cos\hat{\theta}\cos\hat{\psi}\cdot\delta\omega_{xv}+(\sin\hat{\phi}\sin\hat{\theta}\cos\hat{\psi}-\cos\hat{\phi}\sin\hat{\psi})\cdot\delta\omega_{yv}+\\
&\qquad+(\cos\hat{\phi}\sin\hat{\theta}\cos\hat{\psi}+\sin\hat{\phi}\sin\hat{\psi})\cdot\delta\omega_{zv}.
\end{aligned} \tag{63}$$

Therefore, the elements of the matrix $\tilde{\tilde{R}}$ from equation (59) are calculated by using relations of the form:

$$\begin{aligned}
&r_{11}=r_{22}=r_{33}=0,\\
&r_{21}=-r_{12}=(\omega_{yl}\delta\phi-\omega_{xl}\delta\theta)-a_{21}+\delta\omega_{zl},\\
&r_{13}=-r_{31}=(\omega_{xl}\delta\psi-\omega_{zl}\delta\phi)-a_{13}+\delta\omega_{yl},\\
&r_{32}=-r_{23}=(\omega_{zl}\delta\theta-\omega_{yl}\delta\psi)-a_{32}+\delta\omega_{xl}.
\end{aligned} \tag{64}$$

Taking into account that:

$$[\delta\vec{\omega}_v]_v=[\delta\omega_{xv},\ \delta\omega_{yv},\ \delta\omega_{zv}]^T, \tag{65}$$

can be quickly demonstrated that the elements described by formulas (63) come from a product by the form $(\overset{\frown}{R}_l^{\,v})^{T}\cdot[\delta\vec{\omega}_v]_v$. Thus, denoting with:

http://dx.doi.org/10.5772/57583

$$[\vec{\Phi}]_l = [\delta\phi,\ \delta\theta,\ \delta\psi]^T \tag{66}$$

the vector having the components equal with the errors of the attitude angles, it appears that:

$$\begin{bmatrix} \omega_{zl}\delta\theta - \omega_{yl}\delta\psi \\ \omega_{xl}\delta\psi - \omega_{zl}\delta\phi \\ \omega_{yl}\delta\phi - \omega_{xl}\delta\theta \end{bmatrix} = -[\vec{\omega}_l \times \vec{\Phi}]_l, \tag{67}$$

and the matrix equation (59) can be transfigured as:

$$[\dot{\vec{\Phi}}]_l = -[\vec{\omega}_l \times \vec{\Phi}]_l - (\hat{R}_l^v)^T \cdot [\delta\vec{\omega}_v]_v + [\delta\vec{\omega}_l]_l, \tag{68}$$

where $\overset{\frown}{(R_l)}^{v\ \ T} \cdot [\delta\vec{\omega}_v]_v$ represents the errors due to gyro measurements in ENU frame, and $[\delta\vec{\omega}_l]_l$ contains the errors of the angular velocities assessment committed by navigation processor. Equation (67) is the differential equation of the attitude error.

To derive the equation that characterizes the speed error evolution in time it starts from relation (8) in which it is considered $\vec{\omega}_N = \vec{\omega}_l$:

$$\vec{f} = \left.\frac{\mathrm{d}\vec{v}}{\mathrm{d}t}\right|_l + \vec{\omega}_l \times \vec{v} + \vec{\Omega} \times \vec{v} - \vec{g}_a. \tag{69}$$

It results:

$$[\dot{\vec{v}}]_l = [\vec{f}]_l + [\vec{g}_a]_l - [(\vec{\omega}_l + \vec{\Omega}) \times \vec{v}]_l = R_v^l \cdot [\vec{f}]_v + [\vec{g}_a]_l - [(\vec{\omega}_l + \vec{\Omega}) \times \vec{v}]_l, \tag{70}$$

that, in the hypothesis of erroneous measurement of accelerations and angular velocities, becomes:

$$[\dot{\hat{\vec{v}}}]_l = \hat{R}_v^l \cdot [\hat{\vec{f}}]_v + [\hat{\vec{g}}_a]_l - [(\hat{\vec{\omega}}_l + \hat{\vec{\Omega}}) \times \hat{\vec{v}}]_l. \tag{71}$$

Thus, the speed error will be:

$$[\delta\dot{\vec{v}}]_l = [\dot{\vec{v}}]_l - [\dot{\hat{\vec{v}}}]_l = R_v^l \cdot [\vec{f}]_v - \hat{R}_v^l \cdot [\hat{\vec{f}}]_v + [\vec{g}_a]_l - [\hat{\vec{g}}_a]_l - \{[(\vec{\omega}_l + \vec{\Omega}) \times \vec{v}]_l - [(\hat{\vec{\omega}}_l + \hat{\vec{\Omega}}) \times \hat{\vec{v}}]_l\}, \tag{72}$$

but, according to formula (45), $R_v^l = (I_3 - \tilde{R}) \cdot \overset{\frown}{R}_v^l$, and we have:

$$\begin{aligned}[\delta\vec{v}]_l &= \hat{R}_v^l \cdot [\delta\vec{f}]_v - \tilde{R} \cdot \hat{R}_v^l \cdot [\vec{f}]_v + [\delta\vec{g}_a]_l - \{[(\vec{\omega}_l + \vec{\Omega}) \times \vec{v}]_l - [(\hat{\vec{\omega}}_l + \hat{\vec{\Omega}}) \times \hat{\vec{v}}]_l\} = \\ &= -[\vec{\Phi}]_l \cdot [\vec{f}]_v + \hat{R}_v^l \cdot [\delta\vec{f}]_v + [\delta\vec{g}_a]_l - [(\vec{\omega}_l + \vec{\Omega}) \times \delta\vec{v}]_l - [(\delta\vec{\omega}_l + \delta\vec{\Omega}) \times \vec{v}]_l,\end{aligned} \tag{73}$$

in which:

$$[\delta\vec{g}_a]_l = [0,\ 0,\ -3{,}08 \cdot 10^{-6} \cdot \delta h] \approx [0,\ 0,\ -2\frac{KM_P}{a^2} \cdot \frac{\delta h}{a}] = [0,\ 0,\ -2\frac{g}{a} \cdot \delta h]. \tag{74}$$

$$[\delta\vec{\Omega}]_l = [0,\ -\Omega \cdot \sin\phi \cdot \delta\phi,\ \Omega \cdot \cos\phi \cdot \delta\phi]^T. \tag{75}$$

Equations (28) give the expressions for the speed components:

$$\begin{aligned}v_{xl} &= (R_\lambda + h) \cdot \cos\phi \cdot \dot{\lambda}, \\ v_{yl} &= (R_\phi + h) \cdot \dot{\phi}, \\ v_{zl} &= \dot{h},\end{aligned} \tag{76}$$

from where are obtained the positioning errors on the axes of the ENU frame:

$$\begin{aligned}\delta x_l &= (R_\lambda + h) \cdot \cos\phi \cdot \delta\lambda, \\ \delta y_l &= (R_\phi + h) \cdot \delta\phi, \\ \delta z_l &= \delta h.\end{aligned} \tag{77}$$

By derivation with respect to time, equations (77) imply:

$$\begin{aligned}\delta\dot{x}_l &= \left[\frac{\partial R_\lambda}{\partial\phi} \cdot \dot{\phi} \cdot \cos\phi - (R_\lambda + h) \cdot \sin\phi \cdot \dot{\phi}\right]\delta\lambda + (R_\lambda + h) \cdot \cos\phi \cdot \delta\dot{\lambda} + \cos\phi \cdot \dot{h} \cdot \delta\lambda, \\ \delta\dot{y}_l &= \frac{\partial R_\phi}{\partial\phi} \cdot \dot{\phi} \cdot \delta\phi + (R_\phi + h) \cdot \delta\dot{\phi} + \dot{h} \cdot \delta\phi, \\ \delta\dot{z}_l &= \delta\dot{h},\end{aligned} \tag{78}$$

and, by differentiating the velocity components (76), we get expressions:

http://dx.doi.org/10.5772/57583

$$\begin{aligned}
\delta v_{xl} &= \left[\frac{\partial R_\lambda}{\partial \phi}\cdot\cos\phi-(R_\lambda+h)\cdot\sin\phi\right]\cdot\dot{\lambda}\cdot\delta\phi+(R_\lambda+h)\cdot\cos\phi\cdot\delta\dot{\lambda}+\cos\phi\cdot\dot{\lambda}\cdot\delta h,\\
\delta v_{yl} &= \frac{\partial R_\phi}{\partial \phi}\cdot\dot{\phi}\cdot\delta\phi+(R_\phi+h)\cdot\delta\dot{\phi}+\dot{\phi}\cdot\delta h,\\
\delta v_{zl} &= \delta\dot{h}.
\end{aligned} \tag{79}$$

Can be easily verified, starting from the expressions of R_λ and R_ϕ, that is valid the formula:

$$\frac{\partial R_\lambda}{\partial \phi}\cos\phi = R_\lambda\cdot\sin\phi - R_\phi\cdot\sin\phi. \tag{80}$$

Thus, relations (78) and (79) become:

$$\begin{aligned}
\delta\dot{x}_l &= (R_\lambda+h)\cdot\cos\phi\cdot\delta\dot{\lambda}-(R_\phi+h)\cdot\sin\phi\cdot\dot{\phi}\cdot\delta\lambda+\cos\phi\cdot\dot{h}\cdot\delta\lambda,\\
\delta\dot{y}_l &= \frac{\partial R_\phi}{\partial \phi}\cdot\dot{\phi}\cdot\delta\phi+(R_\phi+h)\cdot\delta\dot{\phi}+\dot{h}\cdot\delta\phi,\\
\delta\dot{z}_l &= \delta\dot{h}
\end{aligned} \tag{81}$$

and

$$\begin{aligned}
\delta v_{xl} &= (R_\lambda+h)\cdot\cos\phi\cdot\delta\dot{\lambda}-(R_\phi+h)\cdot\sin\phi\cdot\dot{\lambda}\cdot\delta\phi+\cos\phi\cdot\dot{\lambda}\cdot\delta h,\\
\delta v_{yl} &= \frac{\partial R_\phi}{\partial \phi}\cdot\dot{\phi}\cdot\delta\phi+(R_\phi+h)\cdot\delta\dot{\phi}+\dot{\phi}\cdot\delta h,\\
\delta v_{zl} &= \delta\dot{h},
\end{aligned} \tag{82}$$

from where we obtain:

$$\begin{aligned}
\delta\dot{x}_l &= \delta v_{xl}-(R_\phi+h)\cdot\sin\phi\cdot[\dot{\phi}\cdot\delta\lambda-\dot{\lambda}\cdot\delta\phi]+\cos\phi\cdot[\dot{h}\cdot\delta\lambda-\dot{\lambda}\cdot\delta h],\\
\delta\dot{y}_l &= \delta v_{yl}+\dot{h}\cdot\delta\phi-\dot{\phi}\cdot\delta h,\\
\delta\dot{z}_l &= \delta v_{zl}.
\end{aligned} \tag{83}$$

One observes that the derivative of the position error on the vertical channel is equal with the speed error.

If we denote:

$$[\vec{p}]_l = [\delta p_x,\ \delta p_y,\ \delta p_z]^T = [-\delta\phi,\ \cos\hat{\phi}\cdot\delta\lambda,\ \sin\hat{\phi}\cdot\delta\lambda]^T, \tag{84}$$

then:

$$[\vec{p}\times\vec{v}]_l=\begin{bmatrix}\cos\phi\cdot\dot{h}\cdot\delta\lambda-(R_\phi+h)\cdot\sin\phi\cdot\dot{\phi}\cdot\delta\lambda\\(R_\lambda+h)\cdot\sin\phi\cdot\cos\phi\cdot\dot{\lambda}\cdot\delta\lambda+\dot{h}\cdot\delta\phi\\-(R_\phi+h)\cdot\dot{\phi}\cdot\delta\phi-(R_\lambda+h)\cdot\cos^2\phi\cdot\dot{\lambda}\cdot\delta\lambda\end{bmatrix}. \tag{85}$$

Also, having in mind the expressions for the angular speed components relative to the ECEF frame $\vec{\omega}_r$ in ENU frame (eq. (14)), it results:

$$[\vec{\omega}_r\times\delta\vec{r}']_l=\begin{bmatrix}\cos\phi\cdot\dot{\lambda}\cdot\delta h-(R_\phi+h)\cdot\sin\phi\cdot\dot{\lambda}\cdot\delta\phi\\(R_\lambda+h)\cdot\sin\phi\cdot\cos\phi\cdot\dot{\lambda}\cdot\delta\lambda+\dot{\phi}\cdot\delta h\\-(R_\phi+h)\cdot\dot{\phi}\cdot\delta\phi-(R_\lambda+h)\cdot\cos^2\phi\cdot\dot{\lambda}\cdot\delta\lambda\end{bmatrix} \tag{86}$$

and, from there:

$$[\vec{p}\times\vec{v}]_l-[\vec{\omega}_r\times\delta\vec{r}']_l=\begin{bmatrix}\cos\phi\cdot(\dot{h}\cdot\delta\lambda-\dot{\lambda}\cdot\delta h)-(R_\phi+h)\cdot\sin\phi\cdot(\dot{\phi}\cdot\delta\lambda-\dot{\lambda}\cdot\delta\phi)\\\dot{h}\cdot\delta\phi-\dot{\phi}\cdot\delta h\\0\end{bmatrix}. \tag{87}$$

With the notation:

$$[\delta\dot{\vec{r}}']_l=[\delta\dot{x}_l,\ \delta\dot{y}_l,\ \delta\dot{z}_l], \tag{88}$$

the equation characterizing the evolution in time of the positioning error (eq. (83)) becomes:

$$[\delta\dot{\vec{r}}']_l=[\delta\vec{v}]_l+[\vec{p}\times\vec{v}]_l-[\vec{\omega}_r\times\delta\vec{r}']_l. \tag{89}$$

In conclusion, the error model of the navigation algorithm in terrestrial non-inertial reference frames by using attitude matrices is described by next equations:

$$\begin{cases}[\dot{\vec{\Phi}}]_l=-[\vec{\omega}_l\times\vec{\Phi}]_l-(\hat{R}_l^v)^T\cdot[\delta\vec{\omega}_v]_v+[\delta\vec{\omega}_l]_l,\\[\delta\dot{\vec{v}}]_l=-[\vec{\Phi}]_l\times[\vec{f}]_v+\hat{R}_v^l\cdot[\delta\vec{f}]_v+[\delta\vec{g}_a]_l-[(\vec{\omega}_l+\vec{\Omega})\times\delta\vec{v}]_l-[(\delta\vec{\omega}_l+\delta\vec{\Omega})\times\vec{v}]_l,\\[\delta\dot{\vec{r}}']_l=[\delta\vec{v}]_l+[\vec{p}\times\vec{v}]_l-[\vec{\omega}_r\times\delta\vec{r}']_l.\end{cases} \tag{90}$$

http://dx.doi.org/10.5772/57583

The resulting model consists of a system of coupled differential equations and contains nine variables: three variables are errors in the determination of the attitude angles ($\delta\phi$, $\delta\theta$, $\delta\psi$), three variables are errors in the determination of the speed (δv_{xl}, δv_{yl}, δv_{zl}), and three variables are errors in determination of the position (δx_l, δy_l, δz_l). The input variables of the model are the errors of the six inertial sensors used in the strap-down inertial navigation system. In addition to the nine variables, in the error model are involved the global positioning errors of the vehicle$\delta\lambda$, $\delta\phi$, δh, linking the nine differential equations. Numerical integration of the error model is rather difficult due to the couplings between its equations, but also due to the time evolution considered for inertial sensors errors. It can be performed, however, some numerical simulations, for different sources of error affecting the inertial sensors, in order to highlight their influence on the final errors of the navigation algorithm.

4. Numerical simulations

The validation of the navigation algorithm and of its error model is achieved by building Matlab/Simulink models for them followed by numerical simulation of these models for several navigation particular cases.

Following is conducted a study of the dependence of the inertial navigator outputs errors by the errors of the used inertial sensors. For this purpose, the Matlab/Simulink models built for acceleration and gyro sensors are used; on the inertial navigator inputs are considered three miniaturized optical integrated accelerometers (MOEMS) and three fiber optic gyros with the associated errors according to their data sheets. Due to the fact that the accelerometer and gyro software developed models allow users to work independently with each sensor error in the theoretical model, are studied the influences of the noise, bias and scale factor sensors errors on the navigation solution components. Simulations are performed for three different navigation cases, the vehicle having the same initial position in all three cases: 1) the vehicle is immobile, 2) the vehicle runs at 0.1 g acceleration on the x-axis, 3) The vehicle is subjected to turning with angular velocity 0.1 degree/s, while running on the track with acceleration 0.1 g along x-axis, which means the sensing of an acceleration of-0.0516 m/s^2 (-0.0053 g) along y-axis.

Thus, starting from the navigation algorithm block scheme in Fig. 3 the Matlab/Simulink model in Fig. 4 is obtained. Also, the software implementation of the navigator error model leads to the Matlab/Simulink model in Fig. 5.

With these two models it results the validation model in Fig. 6; “REAL” and “IDEAL” are blocks modelling the navigation algorithm (as in Fig. 4), having as inputs accelerations and angular speeds signals disturbed by the errors of strap-down inertial sensors, respectively undisturbed by the errors of strap-down inertial sensors. “ERROR” is a block by the form in Fig. 5. The input blocks “Acc” and “Gyro” are accelerometers and gyros models as in Fig. 1 and Fig. 2, and theirs outputs are applied to the “REAL” block. The values of the input constants are considered to be ideal signals, un-disturbed by the acceleration and rotation sensors, these being applied to the “IDEAL” block.

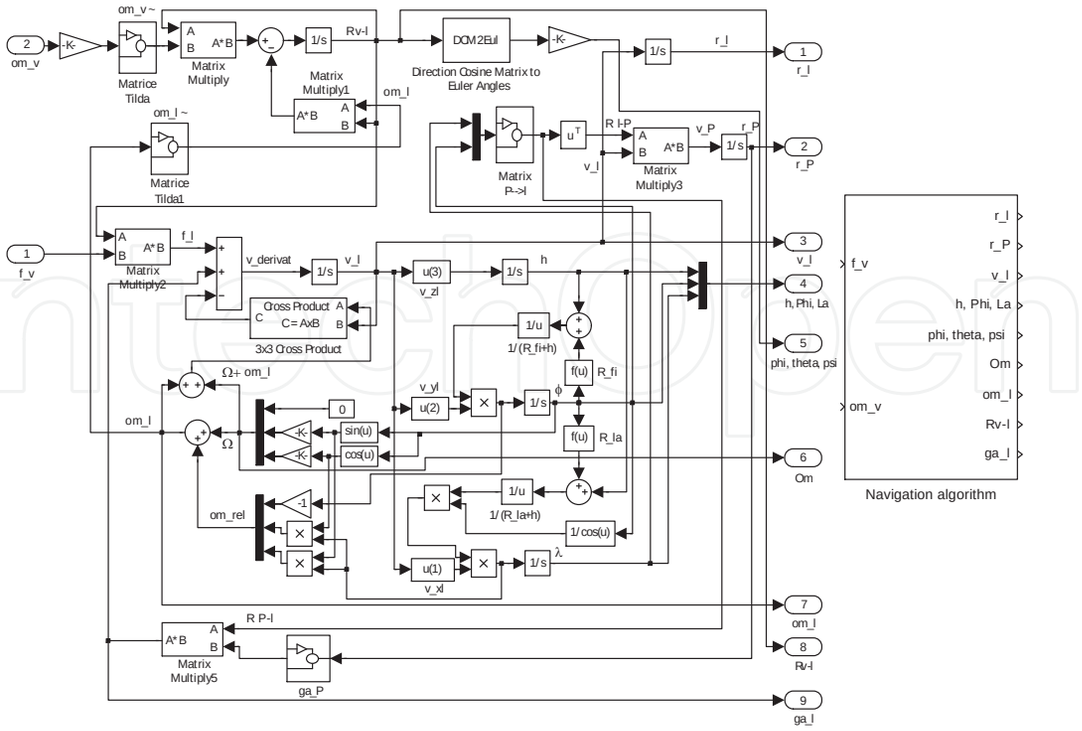

Figure 4. Matlab/Simulink model of the navigation algorithm.

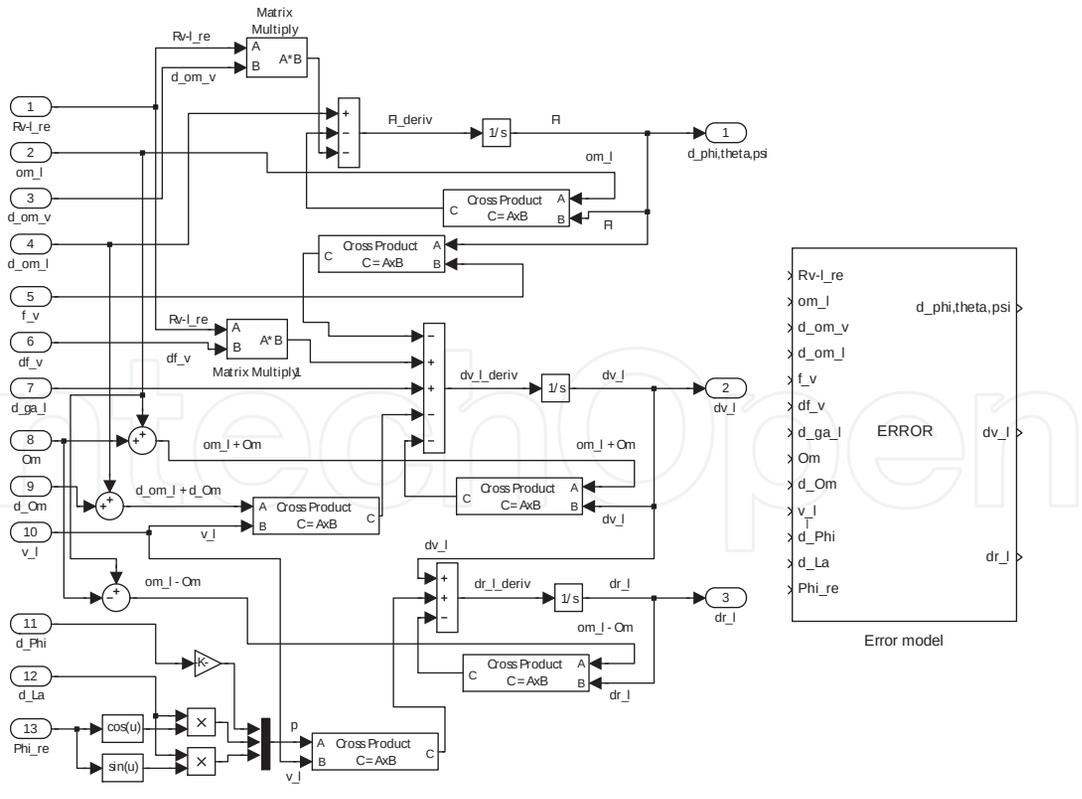

Figure 5. Matlab/Simulink implementation of the inertial navigator error model.

http://dx.doi.org/10.5772/57583

The error model validation is realized through the comparison of the differences between the outputs of the "IDEAL" and "REAL" blocks with the outputs of the error model. In Fig. 7 a. are depicted the attitude angles errors, the first column containing the differences between the outputs of the "IDEAL" and "REAL" blocks, and the second column-the outputs of the error model. In the same mode are built Fig. 7 b. (for the positioning errors in ENU reference frame) and Fig. 7 c. (for the speed errors in ENU reference frame).

The reading errors of the accelerometers (δf_{xv}, δf_{yv}, δf_{zv}) and of the gyros ($\delta\omega_{xv}$, $\delta\omega_{yv}$, $\delta\omega_{zv}$) applied at the error model inputs are presented in Fig. 8. For the accelerometers were neglected the effects of the cross-axis accelerations, while for the gyros were neglected the effects of the sensitivity to the accelerations; the data for three miniaturized optical integrated accelerometers (MOEMS) and three fiber optic gyros were used in sensors models.

The un-disturbed inputs were null on all rotation axes and on the *x* and *y* axes of acceleration, while for the *z* channel of acceleration the input was the local gravitational acceleration.

Analysing the error curves in all of the three parts of Fig. 7 can be easily concluded that the allures of the curves in the first columns are similarly with the allures of the curves in the second columns. As a consequence, the error model described by the equations (90) characterizes precisely the deviations of the attitude angles, and of the vehicle coordinates and speeds in ENU frame from their right values, free of the inertial sensors errors influence. On the other way, we can observe that the errors appearing in the altitude channel are much bigger than the errors in the two horizontal channels, and the attitude angles errors are comparable as values in all of the three channels, having an oscillatory behaviour.

For the next steps of the numerical study, just the outputs of the error model in Fig. 6 are considered. As we already mention, simulations are performed for three different navigation cases, starting from the same initial position: 1) the vehicle is immobile, 2) the vehicle runs at 0.1 g acceleration in the North (x-axis) 3) The vehicle is subjected to turning with angular velocity 0.1 degree/s, while running on the track with acceleration 0.1 g along x-axis, which means the sensing of an acceleration of-0.0516 m/s^2 (-0.0053 g) along y-axis.

For the first case, the curves in Fig. 9 are obtained and the absolute maximal values of the attitude, position and speed errors in Table 1.

According to the graphical characteristics and to the numerical results presented in Table 1, the errors of the accelerometers and gyros scale factors have an insignificant weight in the increase of the attitude angles errors, accelerometers biases cause an increase with 0.26% percent of the roll and pitch angles errors and not affect the yaw angle error, and gyros biases have important weights in all attitude angles errors, producing an increase with 76.78% in roll angle error, with 95.52% in the pitch angle error and with 149.5% in the yaw angle error. Considering simultaneously the biases and scale factor errors at accelerometers produces an increase with 0.2432% of the error in the roll channel and with 0.26% in the pitch channel, while the error in the yaw channel in approximately constant. Can be observed that the combination of the two accelerometers errors with the noise has beneficial effects in the roll channel by

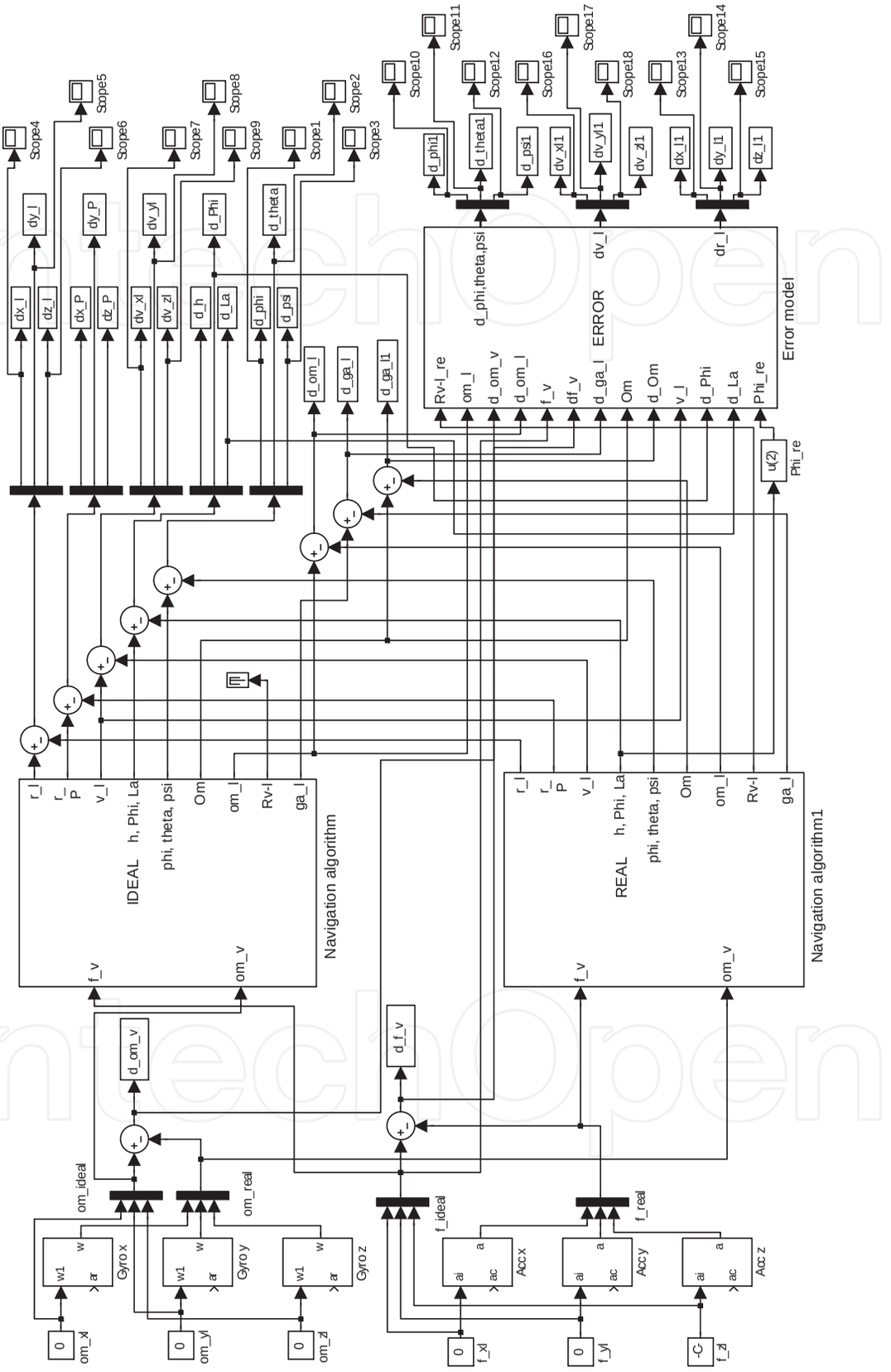

Figure 6. Matlab/Simulink validation model.

http://dx.doi.org/10.5772/57583

limiting the growth of error, compared to the situation in which is present only the bias. Proceeding similar for the gyros, the effect of the simultaneous considering of bias and scale factor errors is reflected by an increase with 76.77% of the error in the roll channel, with 95.52% in the pitch channel and with 149.5% in the yaw channel. Analysing the results obtained when all errors of the inertial sensors in IMU are taken into account, can be noticed an increase with 77.02% of the roll angle error, with 96.12% of the pitch angle error and with 149.5% of the yaw angle error. As a conclusion, the attitude angles errors are decisive influenced by the gyros biases (the strongest in the yaw channel), in a small degree by the accelerometers biases (in the roll and pitch channels) and negligible by the accelerometers and gyros scale factor errors.

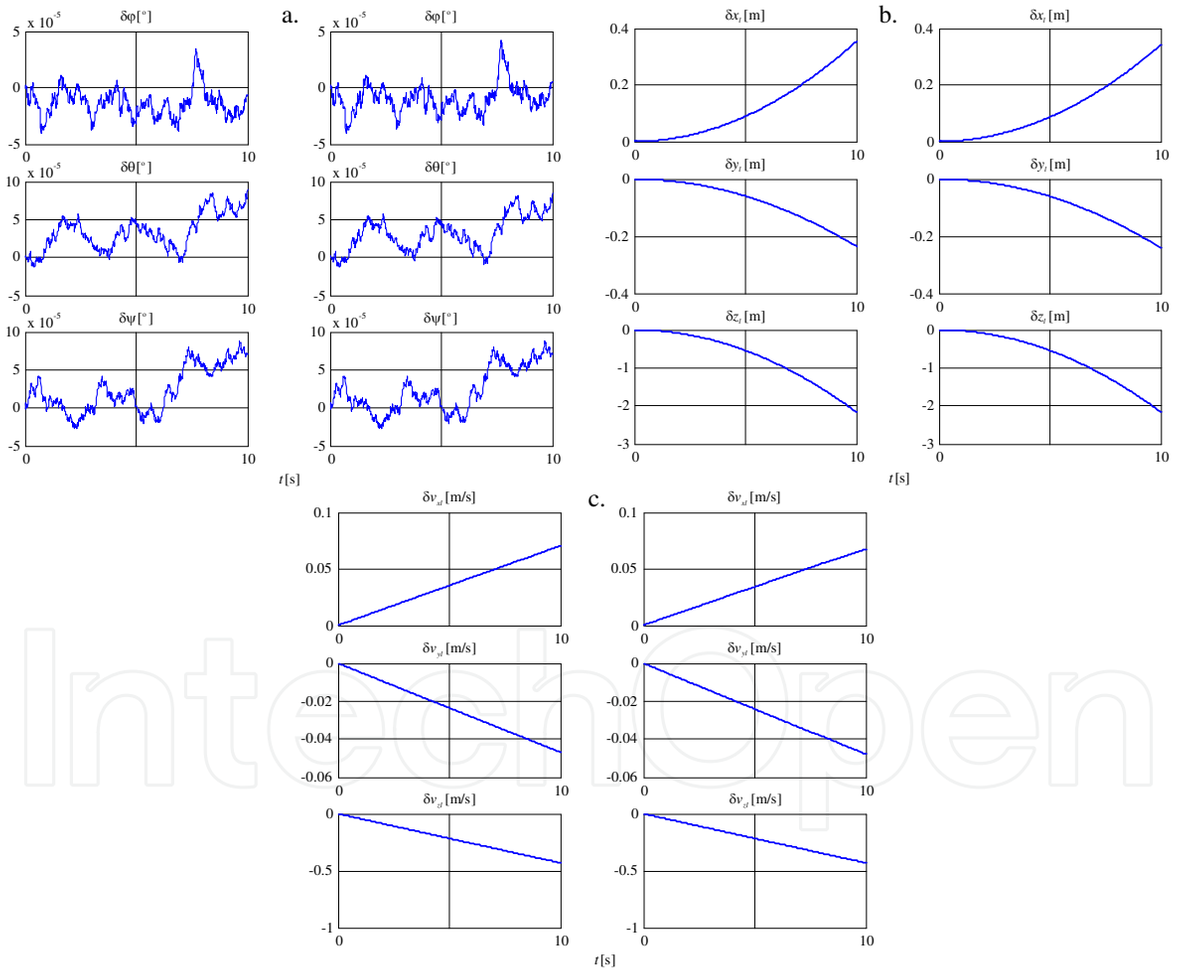

Figure 7. Errors of attitude angles, positioning and speed at validation.

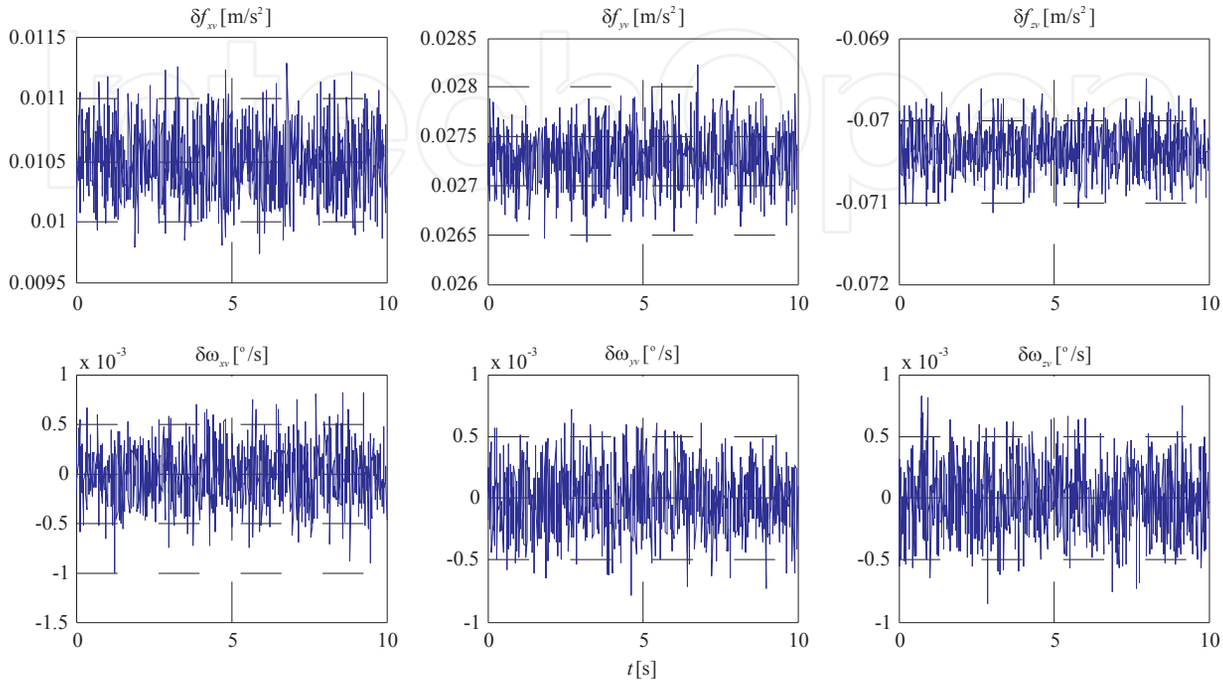

Figure 8. Reading errors of the accelerometers and of the gyros.

Sensors errors	Attitude angles errors [°]			Position errors [m]			Speed errors [m/s]		
	$\delta\varphi$	$\delta\theta$	$\delta\psi$	δx_l	δy_l	δz_l	δv_{xl}	δv_{yl}	δv_{zl}
All null (just noise)	$3.6132\cdot10^{-4}$	$1.5614\cdot10^{-4}$	$1.5281\cdot10^{-4}$	1.0329	2.0788	17.6175	0.0321	0.0984	0.5878
$B_{Acc}\neq 0$	$3.6226\cdot10^{-4}$	$1.5654\cdot10^{-4}$	$1.5281\cdot10^{-4}$	11.688	6.4823	28.2643	0.3937	0.1876	0.943
$\Delta K_{Acc}\neq 0$	$3.6132\cdot10^{-4}$	$1.5614\cdot10^{-4}$	$1.5281\cdot10^{-4}$	1.033	2.079	67.0058	0.0321	0.0984	2.2356
$B_{Acc}\neq 0$ & $\Delta K_{Acc}\neq 0$	$3.6221\cdot10^{-4}$	$1.5654\cdot10^{-4}$	$1.5281\cdot10^{-4}$	11.6629	6.3902	77.6825	0.3929	0.1846	2.5918
$B_{Giro}\neq 0$	$6.3875\cdot10^{-4}$	$3.0529\cdot10^{-4}$	$3.8127\cdot10^{-4}$	2.503	4.0711	17.6175	0.1028	0.1981	0.5878
$\Delta K_{Giro}\neq 0$	$3.6132\cdot10^{-4}$	$1.5614\cdot10^{-4}$	$1.5281\cdot10^{-4}$	1.0328	2.0788	17.6175	0.0321	0.0984	0.5878
$B_{Giro}\neq 0$ & $\Delta K_{Giro}\neq 0$	$6.3874\cdot10^{-4}$	$3.0529\cdot10^{-4}$	$3.8127\cdot10^{-4}$	2.503	4.0711	17.6175	0.1028	0.1981	0.5878
All non-null	$6.3964\cdot10^{-4}$	$3.0623\cdot10^{-4}$	$3.8127\cdot10^{-4}$	10.1927	4.3979	77.6825	0.3195	0.0981	2.5918

Table 1. Absolute maximal values of the attitude, position and speed errors for first navigation case.

http://dx.doi.org/10.5772/57583

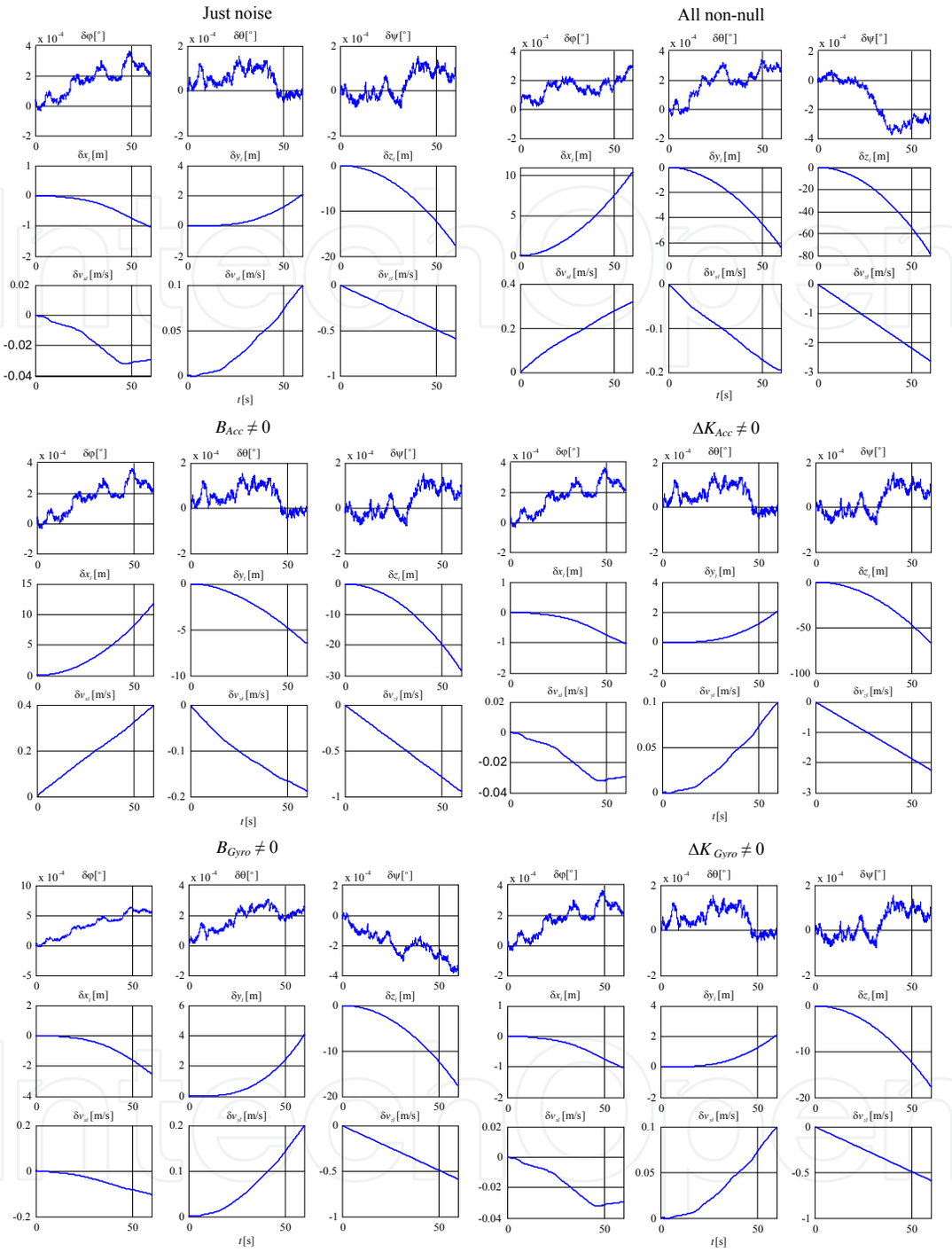

Figure 9. Simulation results for the first navigation case.

Regarding the positioning errors we can observe that: the scale factor error of gyros does not produce any increase in the errors of the three channels; the accelerometers scale factor error influences negligible the errors increase in the horizontal channels (with 0.00968% in x channel and with 0.00962% in y channel) and influences strongly the increase of the vertical channel error (with 280.33%); the accelerometers bias influences strongly the increase of the errors in

horizontal channels (with 1031.57% in x channel and with 211.82% in y channel) and with 60.43% in the vertical channel; the gyros bias does not affect the error in vertical channel but has an important influence regarding the increase of the errors in horizontal channels (with 142.32% in x channel and with 94.39% in y channel); the simultaneous considering of the bias and of the scale factor error for the accelerometers has as result an increase of the error with 1029.14% in x channel, with 207.39% in y channel and with 340.93% in vertical channel (it is noted a beneficial effect of the combination of the two errors in the presence of noise, but only in the horizontal channels, in the vertical channel a negative effect is achieved in this regard); the simultaneous considering of the bias and of the scale factor error for the gyros has as result an increase of the error with 142.32% in x channel and with 94.39% in y channel, and does not affect the value of the error in vertical channel; the simultaneous considering of all errors of the inertial sensors in IMU leads to the errors increases with 886.8% in x channel, with 111.55% in y channel and with 340.93% in vertical channel (it is noted a beneficial effect of the combination of all errors in the presence of noise, but only in the horizontal channels, in the vertical channel, keeping the results obtained when all errors of accelerometers were taken into account). Therefore, the positioning errors are negligibly influenced by the scale factor errors of the sensors in IMU, excepting a strong influence on the vertical channel induced by the accelerometers scale factor errors (280.33%), the accelerometers biases have strong influences on all channels (the biggest is on x channel (1031.57%)), and the gyros biases have strong influences on the horizontal channels while in the vertical channel theirs effects are negligible.

For the second navigation case, are considered the taxiing of aircraft in which it is mounted the inertial navigator, starting from the same initial position and the same conditions of speed and attitude as in the first case, with the acceleration of 0.1 g along the x axis. With this case the aim is to study the influence of sensor errors in the navigator errors when on one of the horizontal axis of the accelerometer is applied a non-zero acceleration. By performing numerical simulations for the same cases of influence of sensor errors, the absolute maximal values of the navigator errors in Table 2 and the graphical characteristics in Fig. 10 are obtained.

Sensors errors	Attitude angles errors [°]			Position errors [m]		
	$\delta\varphi$	$\delta\theta$	$\delta\psi$	δx_1	δy_1	δz_1
All null (just noise)	$3.6130\cdot10^{-4}$	$1.5608\cdot10^{-4}$	$1.5284\cdot10^{-4}$	2.7912	2.0834	17.5142
$B_{Acc}\neq 0$	$3.6220\cdot10^{-4}$	$1.5649\cdot10^{-4}$	$1.5284\cdot10^{-4}$	9.9327	6.4778	28.1575
$\Delta K_{Acc}\neq 0$	$3.6130\cdot10^{-4}$	$1.5619\cdot10^{-4}$	$1.5284\cdot10^{-4}$	0.7522	2.068	66.9016
$B_{Acc}\neq 0$ & $\Delta K_{Acc}\neq 0$	$3.6220\cdot10^{-4}$	$1.5660\cdot10^{-4}$	$1.5284\cdot10^{-4}$	13.4510	6.4012	77.5747
$B_{Giro}\neq 0$	$6.3879\cdot10^{-4}$	$3.0516\cdot10^{-4}$	$3.8113\cdot10^{-4}$	4.2608	4.3299	17.3668
$\Delta K_{Giro}\neq 0$	$3.6130\cdot10^{-4}$	$1.5608\cdot10^{-4}$	$1.5284\cdot10^{-4}$	2.7912	2.0834	17.5142
$B_{Giro}\neq 0$ & $\Delta K_{Giro}\neq 0$	$6.3879\cdot10^{-4}$	$3.0516\cdot10^{-4}$	$3.8113\cdot10^{-4}$	4.2608	4.3299	17.3668
All non-null	$6.3969\cdot10^{-4}$	$3.0636\cdot10^{-4}$	$3.8113\cdot10^{-4}$	11.9814	4.1546	77.4273

Table 2. Absolute maximal values of the attitude and position errors for the second navigation case.

http://dx.doi.org/10.5772/57583

Comparing the numerical results in Table 2 with those in Table 1 it can be seen that the percentage of errors influences are almost the same, the only noticeable change being that of accelerometers and gyros biases effect on the positioning error in x channel.

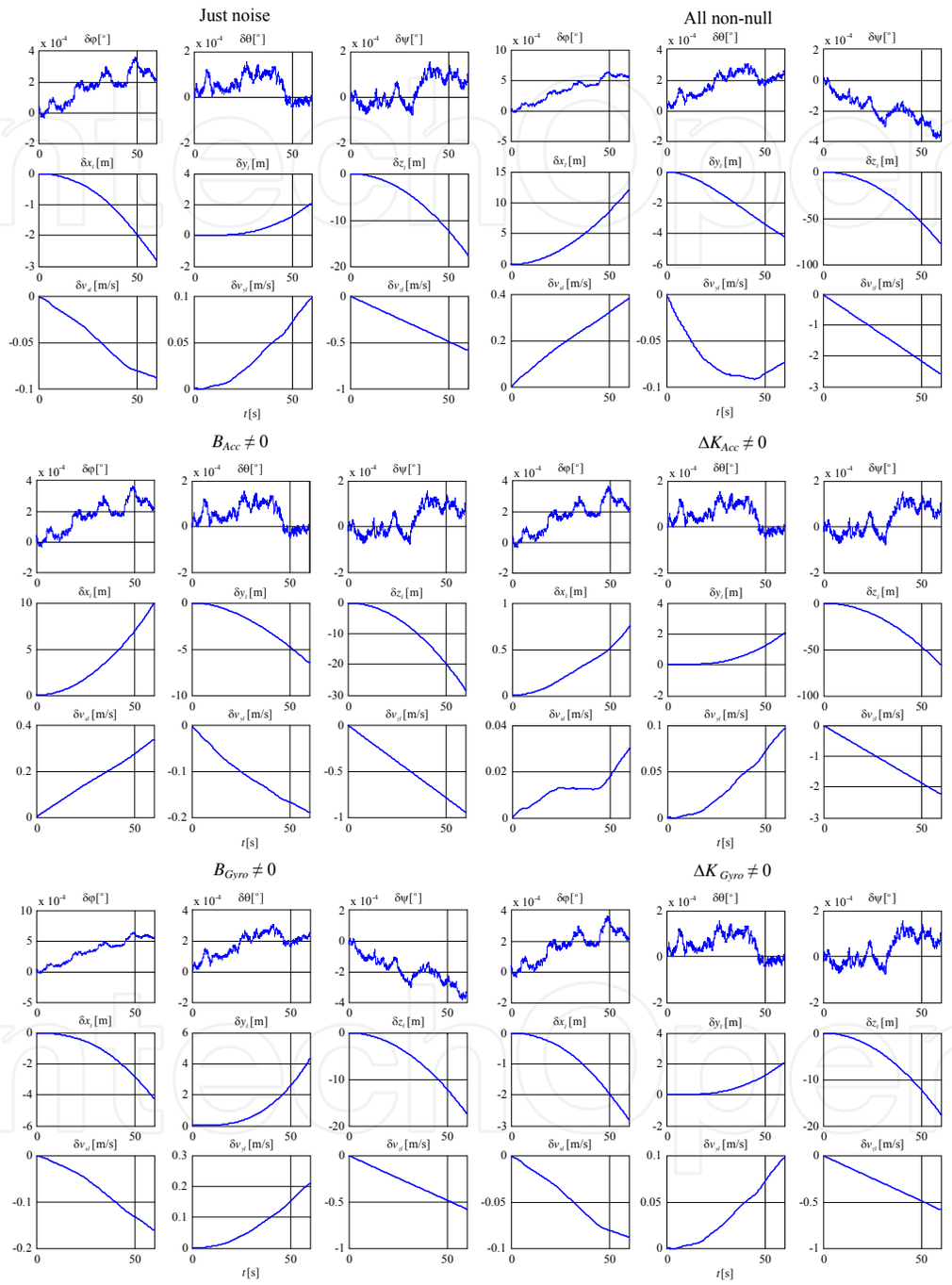

Figure 10. Simulation results for the second navigation case.

It notes, also, the effect of non-zero entry in acceleration, on the x axis of the navigator, on the change of the weights held by the accelerometers scale factor errors in the calculus of the position errors.

Subjecting the vehicle to a gyration angular speed of 0.1°/s, while running on the track with the acceleration 0.1 g along the *x* axis, it has a change of the heading angle of 6 degrees after 1 min and a lateral deviation of 185.4039 m a distance of 1764 m on the East direction. Because the speed is close to the take-off limit, the motion is equivalent to the horizontal movement on a circular arc with a radius of about 16.907 km, which means the sensing of an acceleration of-0.0516 m/s^2 (-0.0053 g) along the *y* axis of the vehicle. Considering the same initial conditions as in the two previous cases, the graphical characteristics of the errors obtained through the numerical simulation are given in Fig. 11, while the absolute maximal values of the navigator errors are shown in Table 3.

Sensors errors	Attitude angles errors [°]			Position errors [m]		
	$\delta\varphi$	$\delta\theta$	$\delta\psi$	δx_l	δy_l	δz_l
All null (just noise)	$3.6773 \cdot 10^{-4}$	$1.6036 \cdot 10^{-4}$	$1.5284 \cdot 10^{-4}$	2.8475	2.1074	17.4978
$B_{Acc} \neq 0$	$3.6823 \cdot 10^{-4}$	$1.6078 \cdot 10^{-4}$	$1.5284 \cdot 10^{-4}$	10.1635	6.0022	28.1410
$\Delta K_{Acc} \neq 0$	$3.6749 \cdot 10^{-4}$	$1.6048 \cdot 10^{-4}$	$1.5284 \cdot 10^{-4}$	0.7238	1.2121	66.8852
$B_{Acc} \neq 0$ & $\Delta K_{Acc} \neq 0$	$3.6832 \cdot 10^{-4}$	$1.6088 \cdot 10^{-4}$	$1.5284 \cdot 10^{-4}$	13.7066	6.8065	77.5581
$B_{Giro} \neq 0$	$6.3662 \cdot 10^{-4}$	$3.1738 \cdot 10^{-4}$	$3.8113 \cdot 10^{-4}$	4.3550	4.3143	17.3350
$\Delta K_{Giro} \neq 0$	$3.6737 \cdot 10^{-4}$	$1.6036 \cdot 10^{-4}$	$1.4694 \cdot 10^{-4}$	2.8472	2.1125	17.4978
$B_{Giro} \neq 0$ & $\Delta K_{Giro} \neq 0$	$6.3662 \cdot 10^{-4}$	$3.1738 \cdot 10^{-4}$	$3.8955 \cdot 10^{-4}$	4.3547	4.3194	17.335
All non-null	$6.3760 \cdot 10^{-4}$	$3.1860 \cdot 10^{-4}$	$3.8955 \cdot 10^{-4}$	12.1993	4.5943	77.3953

Table 3. Absolute maximal values of the attitude and position errors for the third navigation case.

From the graphic and numeric results, it is found the maintaining approximately constant of the final percentages of influence in the navigator error even if the acceleration is not zero in the all three axes of the vehicle, and the angular speed is non-zero on the *z* axis. Also, can be observed the exercise of a stronger influence on the navigator *y* axis by the scale factor error of accelerometer *y*, even the acceleration applied to this axis is the smallest. The big value of the percent (-42.84%) is due to the higher negative value of the scale factor error of accelerometer *y* (-1.08%) comparatively with the other two accelerometers (-0.2% on *x* axis, and 0.28% on *z* axis) (see Table 4). Having non-zero angular speed on the z axis, can be seen a small influence of gyros scale factor errors in yaw channel.

Sensors	Bias			Scale factor error		
	x Axis	*y* Axis	*z* Axis	*x* Axis	*y* Axis	*z* Axis
Gyros	$5.64 \cdot 10^{-6}$ ∘ / s	$4.2 \cdot 10^{-6}$ ∘ / s	$-7.2 \cdot 10^{-6}$ ∘ / s	$-4.056 \cdot 10^{-4}$%	$-3.12 \cdot 10^{-4}$%	$-1.456 \cdot 10^{-4}$%
Acc.	−0.00709128 m/s^2	0.00472752 m/s^2	0.0059094 m/s^2	−0.2 %	−1.08 %	0.28 %

Table 4. Bias and scale factor error for inertial sensors used in simulations.

Assessing the positioning errors in differences relative to the situation when it is considered only the sensors noise, it is observed that the influence of the sensors errors is approximately

http://dx.doi.org/10.5772/57583

the same for the three simulated cases. The errors combining in the general case compared to particular cases, in which are studied the influences of each sensor error, is explained by positive and negative values of the parameters found in Table 4, but also by the crossings in the positive and negative area of the error characteristics in Fig. 9. Also, the high values of position errors in the vertical channel are due largely to the presence of 1g acceleration on the z axis of the navigator, amplifying in this way the errors of the accelerometer in this channel.

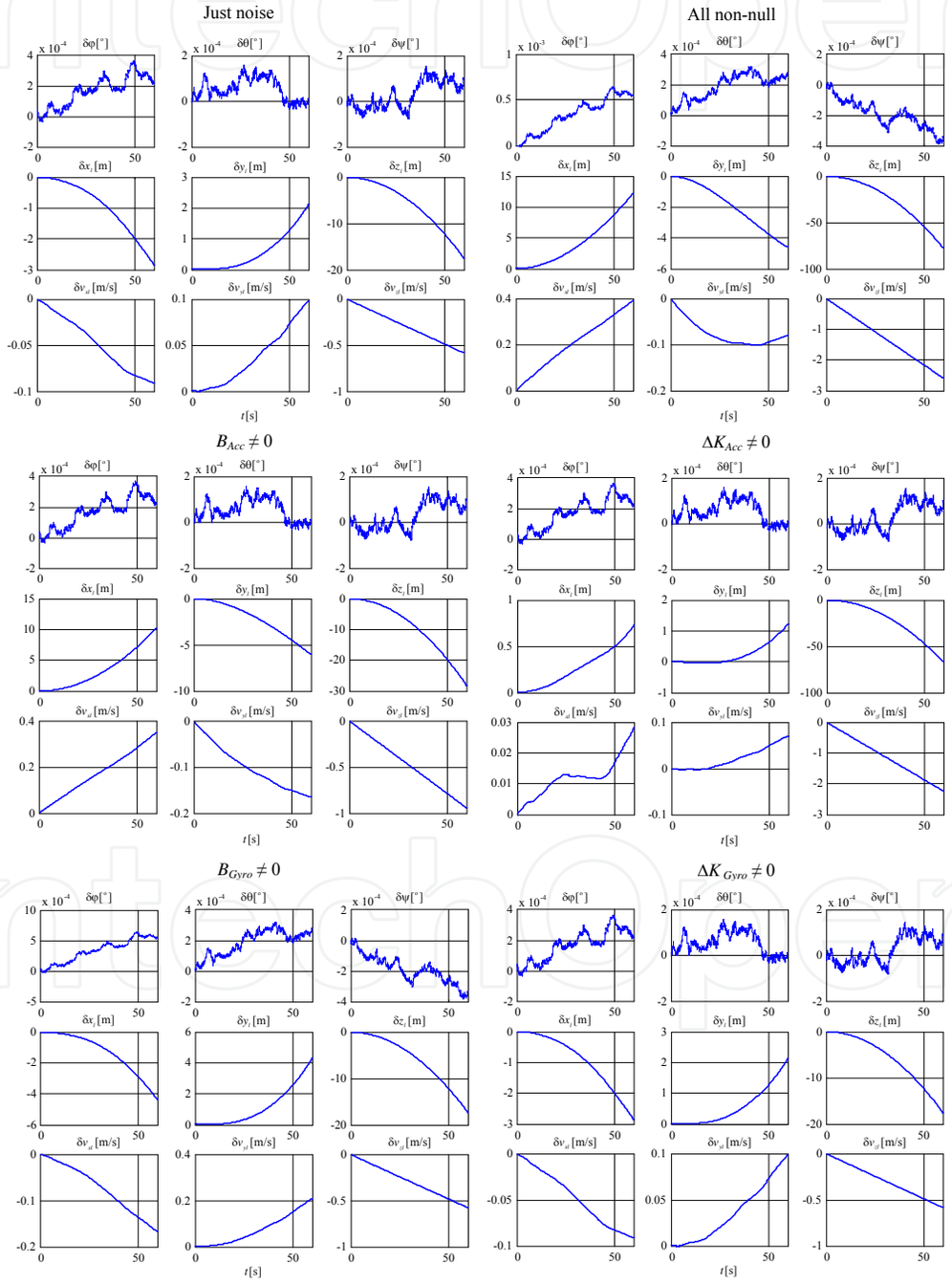

Figure 11. Simulation results for the third navigation case.

5. Conclusions

The numerical simulation of the influences of the inertial sensors errors on the solution of navigation of strap-down inertial navigator was here presented. To perform the simulations some Matlab/Simulink models for the acceleration and rotation sensors based on the sensors data sheets and on the IEEE equivalent models for the inertial sensors were realized. Also, the solving of a navigation problem relative to terrestrial non-inertial reference frames and the development of an error model for the navigator were achieved. The validation of the navigation algorithm and of its error model was realized by building Matlab/Simulink models for them, followed by numerical simulation of these models for several navigation particular cases. Following, a study of the dependence of the inertial navigator outputs errors by the errors of the used inertial sensors was conducted. Simulations were made for three different navigation cases, the vehicle having the same initial position in all three cases: 1) the vehicle is immobile, 2) the vehicle runs at 0.1 g acceleration on the *x*-axis, 3) The vehicle is subjected to turning with angular velocity 0.1 degree/s, while running on the track with acceleration 0.1 g along *x*-axis, which means the sensing of an acceleration of-0.0516 m/s2 (-0.0053 g) along *y*-axis.

The methodology presented here can be used successfully to estimate the effects of the sensors errors on the solution of navigation precision since in the design phase of the inertial navigator, without a prior acquisition of inertial sensors, and based only on their data sheet.

Author details

Teodor Lucian Grigorie[1] and Ruxandra Mihaela Botez[2]

1 University of Craiova, Romania

2 École de Technologie Supérieure, Canada

References

[1] Bekir, E. (2007). *Introduction to Modern Navigation Systems*, World Scientific Publishing Co. Pte. Ltd., ISBN-10: 9812707662, USA, 2007

[2] Bose, P. (2008). *Modern Inertial Sensors and Systems*, Prentice-Hall, ISBN-13: 978-8120333536, India, 2008

[3] Barbour, N., Hopkins, R., Kourepenis, A. & Ward, P. (2010). Inertial MEMS System Applications, NATO RTO Lecture Series, RTO-EN-SET-116, Low-Cost Navigation Sensors and Integration Technology, March 2010

[4] Barbour, N. & Schmidt, G. (2001) Inertial Sensor Technology Trends, *IEEE Sensors Journal*, Vol. 1, No. 4, pp. 332-339, 2001

[5] Barbour, N. (2010). Inertial Navigation Sensors, NATO RTO Lecture Series, RTO-EN-SET-116, Low-Cost Navigation Sensors and Integration Technology, March 2010

[6] Dahia, K. (2005). *Nouveles methodes en filtrage particulaire. Application au recalage de navigation inertielle par mesures altimetriques*, Office National d'Etudes et de Recherches A ´erospatiales (ONERA), Universite Joseph Fourier, These du Doctorat, France, 4 Jan. 2005

[7] Divakaruni, S. & Sanders S. (2006). Fiber optic gyros – a compelling choice for high accuracy applications, 18th International Conference on Optical Fiber Sensors, Cancun, Mexico, October 2006

[8] Dumke, R. & Mueller, T. (2010). Technology with Cold Atoms. *Innovation*, Vol. 9, No. 2, 2010

[9] Edu, I.R., Obreja, R. & Grigorie, T.L. (2011). Current technologies and trends in the development of gyros used in navigation applications – a review, Conference on Communications and Information Technology (CIT-2011), July, 14-16, Corfu, Greece, pp. 63-68, 2011

[10] Farrell, J. (2008). *Aided Navigation: GPS with High Rate Sensors*, McGraw-Hill, ISBN: 978-0-07-149329-1, USA, 2008

[11] Grewal, M. S., Andrews, A. P. & Bartone, C. (2013). *Global navigation satellite systems, inertial navigation, and integration*, John Wiley & Sons, ISBN-13: 978-1118447000, USA, 2013

[12] Grigorie, T. L., Hiliuta, A., Botez, R. M., Aron, I. (2006). Étude numérique et expérimentale d'un algorithme d'attitude pour un système inertiel à composantes liés. *Transactions of the Canadian Society of the Mechanical Engineering (CSME)*, Vol. 30(3), pp. 429-442, ISSN: 0315-8977, 2006

[13] Grigorie, T. L. (2007). *Strap-Down Inertial Navigation Systems. Optimization studies*. Sitech, ISBN: 978-973-746-723-2, Craiova, Romania, 2007

[14] Grigorie, T. L., Lungu, M., Edu, I. R. & Obreja, R. (2010 a). Concepts for error modeling of miniature accelerometers used in inertial navigation systems, *Annals of the University of Craiova, Electrical Engineering series*, Vol. 34, pp. 212-219, ISSN: 1842-4805, 2010

[15] Grigorie, T. L., Lungu, M., Edu, I. R. & Obreja, R. (2010 b). Concepts for error modeling of miniature gyros used in inertial navigation systems, Proceedings of the IEEE International Conference on Mechanical Engineering, Robotics and Aerospace (ICMERA 2010), Bucharest, Romania, December 2-4, 2010

[16] Grigorie, T. L., Lungu, M., Edu, I. R. & Obreja, R. (2010 c). Analysis of the Miniaturized Inertial Sensors Stochastic Errors with the Allan Variance Method: A Review,

Proceedings of the International Conference of Aerospace Sciences "AEROSPATIAL 2010", Section 5, pp. 1-10, ISSN 2067-8622, Bucharest, 20-21 October, 2010

[17] Grigorie, T. L., Botez, R. M., Lungu, M., Edu, I. R. & Obreja, R. (2012 a). MEMS Gyro Performance Improvement through Bias Correction over Temperature using an Adaptive Neural Network trained Fuzzy Inference System, *Proceedings of the Institution of Mechanical Engineers, Part G: Journal of Aerospace Engineering*, September 2012, Vol. 226(9), pp. 1121-1138, ISSN: 0954-4100, 2012

[18] Grigorie, T. L., Obreja, R., Sandu, D. G., Corcau, J. I. (2012 b). Allan variance analysis of the miniaturized sensors in a strap-down inertial measurement unit, 12th International Multidisciplinary Scientific GeoConference - SGEM2012, ISSN 1314-2704, Vol. 3, pp. 443 – 450, June 17-23, 2012

[19] Hopkins, R., Barbour, N., Gustafson, D.E. & Sherman, P. (2010). Miniature Inertial and Augmentation Sensors for Integrated Inertial/GPS Based Navigation Applications, NATO RTO Lecture Series, RTO-EN-SET-116, Low-Cost Navigation Sensors and Integration Technology, March 2010

[20] Kraft, M. (2000). Micromachined inertial sensors: The state-of-the-art and a look into the future, *Meas. Control*, vol. 33, no. 6, pp.164 -168, 2000

[21] KVH Industries Inc. (2007). *An update on KVH fiber optic gyros and their benefits relative to other gyro technologies*, March 2007

[22] Lawrence, A. (1998). *Modern Inertial Technology: Navigation, Guidance and Control* – Second Edition, Springer Verlag, New York, ISBN: 978-1-4612-7258-8, 1998

[23] Pavlath, G. (2006). Fiber Optic Gyros: The Vision Realized, 18th International Conference on Optical Fiber Sensors, Cancun, Mexico, October 2006

[24] Radix, J.C. (1993). *Systemes inertiels a composants lies <<Strap-Down>>, Cepadues-Editions*, Ecole Nationale Superieure de l'Aeronautique et de l'Espace SUP'AERO, Toulouse, France

[25] Salychev, O. S. (1998). *Inertial Systems in Navigation and Geophysics*, Bauman MSTU Press, ISBN: 5703813468, Moscow, Russia, 1998

[26] Savage, P. G. (2000). *Strapdown Analytics, Part 1.* Strapdown Associates, Inc., ISBN: 9780971778603, USA, 2000

[27] Schmidt, G. (2010). INS/GPS Technology Trends, NATO RTO Lecture Series, RTO-EN-SET-116, Low-Cost Navigation Sensors and Integration Technology, March 2010

[28] Tawney, J., et al. (2006). Photonic Crystal Fiber IFOGs, Optical Society of America 18th International Conference on Optical Fiber Sensors, Cancun, Mexico, October 2006

[29] Titterton, D. H. & Weston, J. (2004). *Strapdown inertial navigation technology - 2nd Edition*, Institution of Engineering and Technology, ISBN: 0 863413587, USA, 2004.